Melt Inclusion Formation Mechanisms and Compositional Effects in High-An Feldspar and High-Fo Olivine in Anhydrous Mafic Silicate Liquids

Edward Kohut
Department of Geosciences, 104 Wilkinson Hall
Oregon State University
Corvallis, OR 97330-5506
kohute@geo.oregonstate.edu
voice: (541) 737-3023
fax: (541) 737-1200

Roger L. Nielsen
Department of Geosciences, 104 Wilkinson Hall
Oregon State University
Corvallis, OR 97330-5506
nielsenr@geo. oregonstate.edu
voice: (541) 737-1235

Abstract Important aspects of melt inclusion formation and potential compositions effects have been addressed through a series of experiments using anorthite/fosterite saturated anhydrous mafic liquids. Experimental charges were cooled from 1300º to 1230º and 1210º C at rates of 1º-10º/min., followed by 0-24 hours isothermal periods. Hopper and skeletal crystal morphologies with variable degrees of completeness developed during the cooling period. Planar overgrowth of these textures during isothermal periods led to the formation of inclusions, the majority of which formed after 6 hours isothermal run time. We suggest that the change in morphologies is related to a decrease in growth rates and changes in dominant growth mechanisms. In general, inclusion compositions were uniform and similar to the host glass, indicating that with the isothermal times required for most inclusions to form, a boundary layer was not entrapped that could be detected within the limits of our analyses.

INTRODUCTION

Glass inclusions in minerals are commonly presumed to represent entrapped samples of the melt from which the mineral formed (Anderson and Wright, 1972; Anderson, 1974; Watson, 1976; Roedder, 1984). Such melt inclusions within early forming phenocrysts are proposed to trap unmodified parental melts. In basaltic lavas, high-An plagioclase and olivine phenocrysts commonly host melt inclusions that might preserve information on the diversity of mantle-derived parental magmas (Sobolev and Shimizu, 1993; Sobolev, 1996; Saal et al., 1998; Nielsen et al., 1995; Sisson and Bronto, 1998; Sours-Page et al., 1999, 2002; Gaetani and Watson, 2002). The high-An plagioclase phenocrysts ($>An_{90}$) in particular can contain large numbers of melt inclusions, up to several hundred in a single 1 cm phenocryst (Sinton et al., 1993; Nielsen et al., 1995; Johnson et al, 1996; Sours-Page et al., 1999). These inclusions are commonly more Mg-rich than any reported MORB glass, and in many cases their major element compositions are consistent with a parental relationship to the host lava (Nielsen et al., 1995; Sours-Page et al., 1999). However, some inclusions in N-MORB phenocrysts are anomalously depleted or enriched in particular major, minor or trace elements (Sinton et al., 1993; Nielsen et al., 1995; Saal et al., 1998; Sours-Page et al., 1999). For example, in a single sample from the Gorda Ridge, La/Sm and Ti/Zr ratios in plagioclase-hosted melt inclusions ranged from <0.25 to 0.83 and from 90 to 1600 respectively, while the Mg#s of the glass remained constant at 70-72 (Nielsen et al., 1995). Compositional diversity in plagioclase-hosted melt inclusions from N-MORB lavas of the Juan de Fuca Ridge was manifested by K_2O contents that varied from 0.01 to 0.4 wt% and Ti/Zr ratios ranging from <100 to 1300 (Sours-Page et al., 1999). Further examples of compositional diversity in MORB high-An feldspar melt inclusions are provided in a detailed description by McNeill and Danyushevsky (1996).

The means of producing such compositional diversity must be considered before melt inclusion compositions can be properly interpreted, and we must establish whether this variability reflects actual diversity in the melt or is the result of either the entrapment process (as proposed by Danyushevsky et al., 2002) or post-entrapment modification. While investigations have been conducted into whether the composition of some melt inclusions could be influenced by either mineral-melt reaction (Nakamura and Shimikita, 1998) or diffusional processes (Michael et al., 2002), the issue of modification due to entrapment has not been adequately addressed.

Although the formation of fluid and silicate melt inclusions has been examined experimentally (e.g. Bodnar and Sterner, 1984; Student and Bodnar, 1996, 1997, 1999), these studies did not address specific primary melt inclusion formation mechanisms for plagioclase in mafic liquids. Presumably, primary inclusions (i.e. those that form while crystals are growing) in high-An feldspar develop from irregularities in crystal morphology that are subsequently sealed (Roedder, 1984). While experiments on plagioclase morphology have been conducted by Lofgren (1974), Corrigan (1982), and Muncill and Lasaga (1987, 1988), these workers did not make a specific connection between morphology and melt inclusion formation. Secondary inclusions, or those formed by dissolution followed by new growth, have been produced in plagioclase by Nakamura and Shimikita (1998). However, this work involved hydrous melt and An_{59} seed crystals and the results are not relevant to the formation of primary high-An plagioclase-hosted inclusions formed during crystallization under anhydrous conditions. Furthermore, no satisfactory mechanism has been proposed for the bands of inclusions observed in plagioclase phenocrysts (Roedder, 1984).

In this paper, we investigate through a series of experiments the mechanisms for melt inclusion formation in high-An plagioclase in MORB. These experiments were designed to determine whether:

a) Primary melt inclusions will form during crystal growth, during either constant cooling or subsequent isothermal crystallization.
b) Inclusions formed in such a manner trap a liquid representative of the host melt.
c) In the case of anorthite, the specific mechanism responsible for the abundant inclusions can be determined.

Anorthite was chosen due to its widespread presence in basaltic lavas and the common occurrence of large numbers of melt inclusions in the mineral in naturally occurring lavas. MORB liquids in equilibrium with high-An feldspar are also saturated in high-Fo olivine (Sinton et al., 1993; Nielsen et al., 1995) and thus lie on the anorthite/forsterite cotectic of the basalt ternary (Osborn and Tait, 1952). For this reason we have configured our experiments to be in equilibrium with both minerals. This has additional benefit in that it also allows us to observe melt inclusion formation in olivine.

Our experiments were run in capsules fabricated from An_{92} feldspar to achieve anorthite saturation and Fo_{92}olivine crystals were added to ensure forsterite saturation. Glass separated

from lava sampled from the Gorda Ridge (D9-2 Davis and Clague, 1987) was used as the starting material. In our previous phase equilibria experiments (Kohut and Nielsen, 2003), temperatures of 1230° and 1210° C were observed to be favorable for producing An>85 feldspar and high Fo olivine in the liquid. As a result, these were used as our run temperatures in the inclusion formation experiments we report here. Although these earlier experiments provided compositional data on the melt and mineral phases, they were not configured to examine the dynamic effects of undercooling and cooling rate.

METHODS

Phenocrysts of An_{93-96} plagioclase from Arenal Volcano in Costa Rica were used for our experimental capsules. These were cut into ~1 cm cubes and a hole ~2 mm in diameter and 3 mm deep was drilled into each capsule to hold the starting powder. The starting powder consisted of ground glass sampled from a Gorda Ridge N-MORB lava (D9-2 – Davis and Clague, 1987). Kilbourne Hole olivine (Fo_{91-92}) was added to ensure olivine saturation. In earlier experiments that used capsules fabricated from feldspar from a different source, the glass in the run products commonly infiltrated into the capsule through fractures and was difficult to distinguish from pre-existing natural glass. Because of this problem, 0.1 wt% ZrO_2 was added to distinguish the products of our experiment from glass derived from the capsule. However, this precaution proved unnecessary, as the glass in the run products remained confined to the hole in the Arenal capsules. The charges were suspended by 0.1 mm platinum wire in a Deltec vertical quench furnace and the oxygen fugacity was set at the QFM buffer using a mixture of H_2 and CO_2 gasses. The experimental charges were held at an initial melting temperature of 1300°C for two hours to saturate the melt in anorthite and fosterite. The temperature was then dropped at cooling rates of 1°/min, 5°/min and 10°/min to run temperatures of 1210° and 1230° C, or ΔTs of 90° and 70°. For a ΔT of 90°, the isothermal run periods were 0 and 6 hrs. For a ΔT of 70°, the run periods were 0, 1, 3, 6 and 24 hrs. An additional experiment at 1230°C was run for 116 hrs with a cooling rate of 1°/min. At the end of the isothermal run time, the experiments were dropped quenched in water.

Run products were analyzed with the Cameca SX-50 electron microprobe at Oregon State University using a beam current of 30nA for glass and feldspar, and 50 nA for olivine and an accelerating voltage of 15kV. For glass, count times were 30s for Fe, 20s for Mg, Al, Si, P, K, Ti and Zr, and 10s for Na, Ca, Cr, and Mn. For feldspar, count times were 10 seconds for all

elements. For olivine, count times were 20s for Fe and Ni, and 10s for Mg, Al, Si, K, Ti, Na, Ca, Cr, and Mn. The basalt glass standard (USNM 113498/1 VG-A99) was run as an unknown and calculations of relative error were performed using measured-true/measured*100. These calculations indicated glass analyses were accurate within ±0.51% for SiO_2, ±0.05% for TiO_2, ±0.25% for Al_2O_3, ±0.17% for FeO*, ±0.03% for MnO, ±0.16% for MgO, ±0.19% for CaO, ±0.16% for Na_2O, ±0.04% for K_2O and P_2O_5.

We used the method of crystal size distribution to estimate the growth rates of our crystals. This method is an empirical statistical technique used to determine the nucleation and growth rates of phases precipitating from a solution. We will not describe theory here, as full discussions of theory and applications to geologic problems are presented by Marsh (1984), Cashman and Marsh (1984), Cashman (1988), Cashman and Ferry (1988), Mangan (1990), Cashman (1993), Higgins (2000) and Garrido et al. (2001).

To perform CSD analyses, crystal lengths were first measured from backscattered electron images (at magnifications of 200-400x) of the run products using the measuring tool in the NIH IMAGE software (available at http://rsb.info.gov/ij/index.html). The accuracy of measurements was a function of image resolution, which affected the ability to distinguish crystal edges. We determined that the edges could be resolved within 2-4 pixels, which corresponded to 0.5-1 μm. Crystal lengths were then corrected to 3-D lengths with the stereological method of Higgins (2000) using his CSD correction software (downloaded from http://wwwdsa.uqac.uquebec.ca / ~mhiggins/csdcorrections.html). The software was then used to produce to determine the volumetric population density, n_v, with the bin size being determined automatically and the number of bins per decade adjusted to provide the smoothest curves. The data were then plotted and linear regressions used to obtain the slope. Trial runs that added or subtracted the small measuring error (described above) did not produce noticeable changes in CSD results.

TERMINOLOGY

We use the following terms in this paper to describe the morphology of plagioclase and olivine crystals. With the exception of the term intergrown texture used for olivine, these morphologic definitions are modified from those used for plagioclase by Lofgren (1974) and for olivine by Donaldson (1976). In all experiments, more than one morphology for each mineral phase was observed. However, there were one or two predominant morphologies and these are the ones noted in Tables 1.

Plagioclase morphology:

Swallowtail (A-Figure1)- tabular crystals with tapering, bifurcated ends. Simple swallowtails may have two tapering projections from either one or both ends while more complex swallowtails may have multiple or very elongate projections or have a fan shape.

Skeletal (B-Figure1)- incomplete, enlongate crystals. Commonly have hollow cores with complete or nearly complete outer faces or an irregular, tapering outline.

Hopper (C and D-Figure1)- preferential growth from corners that results in a boxy cellular texture that includes indentations or hoppers in the crystals outer surface. This morphology is commonly observed in two dimensions as hook-shaped features. Simple hoppers appear as skeletal crystals with enhanced corner growth. Blocky hoppers show a combination of planar and hopper morphology. Complex hoppers have multiple re-entrants and a variety of forms, from angular to a combination of angular and rounded surfaces. Stepwise growth may also form hoppers along very large crystals or the capsule wall.

Equant and Tabular (E-Figure 1)- euhedral crystals that are equal or near equal in each direction are equant. Tabular crystals are elongated on one axis relative to the others. Inclusions may be present.

Olivine morphology:

Granular (Figure 2a)- anhedral, and subspherical crystals. Either complete or with round, oval or lobate inclusions.

Hopper (Figure 2b)- combination of planar faces, smooth curvilinear lobes and re-entrants. May be complete or highly skeletal. Simple hoppers are granular crystals with curvilinear or planar lobes or C-shape crystals. More elongate hoppers have a hook shape, while complex hoppers have multiple lobes, embayments and a variety of curvilinear and planar faces.

Polyhedral- euhedral equant or tabular crystals with planar faces. This may be either solid or with small inclusions.

Intergrown- small, ~5-15 m anhedral olivine intergrown with plagioclase.

RESULTS

Crystal Morphology

Plagioclase

Feldspars that grew during cooling had skeletal and swallowtail morphologies, and these were more elongate and incomplete following cooling to 90º ΔT than to 70º ΔT . We observed a progression in plagioclase morphology of swallowtail+skeletal→hopper→equant + tabular forms with increasing isothermal run time (Table 1). Multiple forms were common in each experiment, and the occurrence of morphologies in the sequence overlapped. Duplicate cooling rate experiments to 70º ΔT produced similar textures. In experiments quenched at 6 hours isothermal time, feldspars in the melt were predominately hoppers and there were stepwise growths of feldspar on the capsule rim. These feldspar hoppers were best developed in experiments that had 5°/min. cooling (Figure 3a). At an isothermal period of 24 hours, feldspars were blocky hoppers and tabular crystals with small inclusions (Figure 3b). These morphologies were similar to those we observed in our phase equilibria experiments, which had run times of 24 hours (Kohut and Nielsen, 2003). As the isothermal run time increased, inclusions rather than open embayments were observed. This observation coincided with the progression from incomplete morphologies to those with planar faces, and indicates that embayments were enclosed as crystallization progressed. The one experiment with 116 hours isothermal time followed 1°/min. cooling and produced a few large (~203-358 x 50-85 μm) feldspar and olivine (~460 x 350 μm) crystals and smaller blocky feldspars.

Olivine

As indicated by the lack of olivine in the run products from the cooling only experiments (i.e. 0 hours isothermal period), this mineral did not nucleate during the cooling period. Olivine was not observed in any experiments with less than 6 hours isothermal time, except for the 3 hour experiment with 10º/min. cooling to a ΔT of 70º. Olivine morphology changed from granular to hopper to intergrown and polyhedral as the isothermal increased past 6 hours (Table 1). We observed that the occurrences of granular and simple hopper morphologies in olivine overlapped. The hopper forms were similar to those described by Faure et al. (2003) for similar cooling rates and degrees of undercooling. The granular crystals are similar to polyhedral crystals produced by Faure et al. (2003) in the respect that their polyhedral crystals also commonly contained central inclusions. Complex hoppers were also observed that were similar to those described by

Jambon et al. (1992) for 71º ΔT. It is probable that some granular crystals initially formed as C-shape hoppers in which the embayment became enclosed as planar growth became dominant with increasing isothermal time.

Crystal Size Distribution and Growth Rate

Growth rates were examined to determine any correlation between morphology and growth rate that would assist in the determination of the dominant growth mechanism. These rates were calculated from slopes of the linear regression lines through the CSD data for each experiment. Due to the small populations involved (15-25 crystals of each phase per experiment), the R^2 values for the trends ranged from 0.5278 to 0.9525, with an average of approximately 0.76. The data however were reliable enough to estimate growth rates and make relative comparisons.

Growth rates were approximately the same during cooling to both 70º and 90º ΔT, but after 6 hours isothermal run times the rates were slightly slower at 90º ΔT compared to 70º ΔT (Table 2). Plagioclase growth rates were most rapid during cooling and became progressively slower as the isothermal periods increased (Figure 4). For example, plagioclase growth rates during 5º/min. cooling to a ΔT of 70º were 1.00 $x10^{-2}$ μm/s, but decreased to 2.01 x 10^{-3}μm/s by 6 hours isothermal run time, and to $9.1x10^{-4}$μm/s by 24 hours. Similar decreases in growth rate with time were observed following 1º/ min. and 10º/min. cooling (Table 2, Figure 4). Overall, plagioclase growth rates were highest following 10º/min. cooling for all isothermal periods. This observation that an increase in cooling rate will lead to an increase in growth rates has been previously reported by Cashman (1993). Estimated olivine growth rates were fairly constant, but were highest following 10º/min. cooling (Table 2). The implied connection of olivine growth rate to cooling rate, despite the lack of olivine nucleation during cooling, is fully addressed in the discussion. As shown by Figure 4, nucleation rates (which are a function of the growth rate) also decreased with increasing run time. For experiments quenched immediately following cooling, 10º/min. cooling produced the highest nucleation rates, and nucleation rates for experiments following 10º/min. cooling remained higher for all isothermal periods, which corresponds to Cashman's (1993) finding that the higher cooling rates have the highest nucleation rates.

Notably, more higher growth and nucleation rates were associated with incomplete hopper and skeletal morphologies, and the decrease in growth rates coincided with the change to more planar equilibrium morphologies. With rapid growth during cooling, the growth rates would exceed the rates for diffusion of components rejected during growth (Lofgren, 1974). For

growth to continue, the crystal had to form projections into the liquid to reduce latent heat and penetrate the boundary layer (Philpotts, 1994). This would result in the development of elongate crystals with varying degrees of incompleteness. With the slower growth rates, crystal growth would be limited by the surface nucleation on the crystal face and diffusion would be sufficient to remove molecules rejected by crystal growth (Lofgren, 1974; Philpotts, 1994). This results in more even, planar crystal shapes.

Inclusion size distribution

Inclusion sizes were determined to examine any correlation to experiment run time or inclusion composition. Sizes were measured using the same strategy as crystal sizes. For size distribution comparisons, the 3-D size of the inclusions and the conversion of area to volume were corrected for with the same correction software used for the CSDs. Although inclusion shapes were variable and commonly asymmetric, most could be approximated as spheres and we had the CSD correction program treat the inclusions as spherical objects. The data produced allowed comparison of relative population densities. These were fairly constant from experiment to experiment, although the size distributions in olivine-hosted inclusions were more consistent. The highest population density occurred in inclusions under 10 μm in plagioclase and 5 μm in olivine (Figure 5). In the 116-hour experiment, the distribution was most heavily weighted towards smaller sizes. This may indicate that as smooth planar morphologies became more dominant with run time, fewer inclusions were produced and early-formed inclusions decreased in size by crystallization of the host along the inclusion walls. In such circumstances, the largest and most easily analyzed inclusions would be those that formed closest to the end of the experiment run time. An inclusion size decrease might have also resulted in the elimination of the earliest formed inclusions.

Inclusion Frequency

The frequency of inclusion occurrence was estimated for each experiment by counting the number of inclusions observed in plagioclase and olivine crystals in the run products and dividing this number by the total number of crystals observed. Due to the fragility of the capsules, we were not able to section them in a consistent manner and the amount of run product and the orientation of the exposed area varied from experiment to experiment. This introduces an uncertain amount of inaccuracy into our frequency estimates. With the limited data we have,

the firmest conclusion we can make is that the majority of inclusions formed with 6 hours or more isothermal time.

A ΔT of 70º appeared to be more favorable for inclusion development than a ΔT of 90º, but cooling rate combined with isothermal run time seemed to exhibit the greatest control on the frequency of melt inclusion occurrence (Table 2). Few plagioclase-hosted inclusions formed during the cooling period (0 hours isothermal time-Table 2). For all isothermal times, the greatest frequency of plagioclase-hosted inclusions followed 5°/min. cooling and increased with longer isothermal periods, peaking at six hours isothermal run time (Table 2). For our experiments, we suggest that 5°/min cooling resulted in more inclusions because with this cooling rate in our system, well-developed hopper textures with many embayments were favored in both the feldspars in the liquid and within the capsule rim overgrowth. However, the number of plagioclase hosted inclusions following 1° and 10°/min cooling was greatest with a 24-hour isothermal period. Since only 0 and 6 hours isothermal periods were used for 90° undercooling, the data for this ΔT were less detailed (Table 2).

As noted earlier, no olivine crystallized during the cooling period and with the exception of 3 hours isothermal time after cooling 10°/min. to 70° ΔT, none appeared with less than 6 hours isothermal time. Consequently, the data on olivine-hosted inclusion frequency were limited to isothermal periods greater than 6 hours. With 6 hours, the greatest number of olivine-hosted inclusions followed 10°/min. cooling to both 70° and 90° ΔT (Table 2). Olivine melt inclusion frequencies at 24 hours isothermal time were fairly similar following cooling at all rates.

Host glass, Inclusion, and Mineral Compositions

In general, liquids quenched during isothermal run periods have compositions that fall along trends towards the natural lava suite (Davis and Clague, 1987) for the starting glass and the starting glass itself. The most notable exceptions are from experiments quenched immediately after cooling; liquids quenched thus had the lowest MgO contents (8.18-9.32%) and had compositions away from the general trends (Table 3 and 4, Figures 6-8). The Al_2O_3 and MgO contents decreased with isothermal time regardless of cooling rate, and these data likely reflect an increasing amount of crystallization with increasing isothermal time. Na_2O, FeO* and TiO_2 contents were similar between experiments with greater than 3 hours isothermal time. The CaO contents were lowest in experiments with 6 hours isothermal time following all cooling rates. The 1 and 3 hour experiments (Table 4) also showed compositional departure from the CaO

trend of the natural lava suite. These data are the probable result of the system not yet being in chemical equilibrium and consequently the melt was still reacting with the capsule and added olivine. The observation that experiments with less than 6 hours isothermal time had not yet crystallized olivine (except for the 3 hour experiment with 10°/min. cooling) is further evidence that the system had yet to achieve equilibrium and the point of multiple saturation. However, the longer period experiments had more time to equilibrate and the glass compositions of all 24-hour experiments regardless of cooling rate were similar (Figure 6-8). The results of the 24-hour experiments also corresponded with the 1230° compositions from our phase equilibria experiments (Kohut and Nielsen, 2003).

Due to the use of a 3 μm beam size for glass analyses, many inclusions were not suitable for EMP analysis. As a consequence, the number of inclusions we have EMP data from (Table 3 and 4) are less than the number of inclusions observed visually. The average inclusion compositions for an experiment are also identical within 2σ and analytical error to the host glass compositions (Table 3 and 4, Figures 6-8). Slow cooling (1°/min.) produced the greatest difference between average melt inclusion and melt compositions: there is a ~0.5-2% difference in Al_2O_3 contents and 0.2-1.2 % variability in MgO between average compositions of host glass and plagioclase-hosted melt inclusions formed during 1°/min. cooling. This diversity may indicate that inclusions in the slow-cooling experiments trapped melt over a wider time interval and at different stages of equilibration (Table 4, Figure 6).

Even though the amounts of compositional difference between host and inclusion compositions were small and within analytical error, it is still possible that what minor diversity there was could be attributed to rejected components trapped within boundary layers surrounding the growing crystals. To test for the presence of such a layer, we compared the sizes of the analyzed inclusions to their compositions. If a layer were entrapped, we would expect to see systematic increases in rejected components with decreasing inclusion sizes, as the smaller inclusions would contain a proportionately greater amount of the boundary layer. Figure 9 illustrates these comparisons, with CaO and Al_2O_3 representing rejected components in olivine-hosted inclusions and Mg# (at% Mg/[Mg+Fe^T]*100) and TiO_2 representing rejected species in plagioclase-hosted inclusions. Although some variability was observed, it was not systematic with size, indicating that the inclusions did not trap discernable boundary layers. Differences between individual inclusion compositions in a given experiment may instead be evidence of

melt being trapped at different stages in equilibration (Figure 9). Note that some individual olivine-hosted inclusions from 6- and 24-hour experiments with 5°/cooling had similar Al_2O_3 contents, even though the averaged inclusion compositions from the experiments were dissimilar (Figure 7). Although inclusions<3-4 μm may have indeed contained compositions that reflected the trapping of a boundary layer, these were too small to be effectively analyzed using EMP. Differences in cations needed for growth by the host crystal were not examined relative to inclusion size due to the uncertainty that could result from the electron beam exciting the same elements in the host crystal, especially in the smallest inclusions. Although such errors would be small, they would be difficult to distinguish from the variability we would be attempting to determine.

The feldspars that crystallized in the run products ranged overall from $An_{83.5}$ to $An_{97.1}$ and the olivines from $Fo_{89.6}$ to $Fo_{93.8}$ (Table 5). Within each experiment, plagioclase compositions were the most variable. The largest feldspars that crystallized during the cooling period or during shorter isothermal periods had 1-5 μm zones of lower An content surrounding a higher An core (Table 5). Zoning was not prevalent in feldspars in experiments quenched after 1 hours isothermal time following 1°/min. cooling, after 3 hours isothermal time following 5°/min. cooling, and after 6 hours isothermal time following 10°/min. cooling. The predicted An content of feldspars in equilibrium with the liquid composition from each experiment was calculated using Equation 1 from Panjasawatwong et al., (1995) and with the Petrolog software program (available at http://www.geol.utas.edu.au/~leonid/Petrolog.html) using the Danyushevsky model and compared to the observed An contents (Table 5, Figure 10). The results suggest that the feldspars that were not in equilibrium (as calculated) with the melt at quench time were also those with incomplete hopper and skeletal morphologies. With longer isothermal times, the prevalence of zoned feldspars diminished and most had overall An contents that were close to equilibrium values.

The compositions of the olivines in the run products were consistently similar to the olivine in the starting material (Fo_{91-92}) and range from $Fo_{89.6-93.8}$ (Table 5). Within each experiment, olivine composition varied only 0.3-0.75 Fo. Chrome spinels were also present in the run products, with Cr#s (at% Cr/[Cr+Al])of 0.32-0.41 and Al_2O_3 contents of 30.0-36.5 wt% . The

presence of spinel indicates that liquid was three-phase (olivine, plagioclase, chromite) saturated at the run temperatures.[1]

DISCUSSION

Inclusion formation mechanisms

The results demonstrate that primary inclusions in high-An feldspar and high-Fo olivine can result from a change in crystal morphology due to a change in growth mechanism similar to the process proposed by Roedder (1984). During the cooling and the initial isothermal periods, feldspars growth rates were several orders of magnitude greater than the estimated ability of diffusion to remove rejected cations or supply those needed for growth. For example, plagioclase grew immediately after 1°/min. cooling at a rate of 1.16×10^{-2} μm/s, while diffusion could only supply Ca at ~1.5×10^{-3} μm/s and remove Fe^{2+} at ~9.5×10^{-7} μm/s (based on diffusion coefficients in Freer, 1981; Cooper et al., 1996). Crystal growth (needed remove latent heat of crystallization during undercooling) could only occur on protuberances through the boundary layer, resulting in swallow-tail and skeletal morphologies with elongate projections (Philpotts, 1994). As growth rates decreased following cooling, the initial result may have been a concentration of growth on crystal corners which resulted in hoppers formed by stepwise growth. As growth rates decreased further with increasing isothermal time, diffusion became more efficient at removing and supplying cations and the growth mechanisms became surface-nucleation controlled. This had the effect of producing more planar crystal faces and tabular and equant morphologies. Embayments from the incomplete morphologies in crystals that grew during undercooling were covered with the planar overgrowth and melt was trapped within the growing crystal.

The results may also provide a potential explanation for the bands of melt inclusions that are commonly observed in plagioclase. During experiments with longer than 3 hours isothermal time, crystals of both olivine and plagioclase nucleated along the capsule rims. The plagioclase in these overgrowths grew in a stepwise fashion to produce hopper textures and these hoppers formed zones of inclusions parallel to the rim (Figure 3a). These zones in the capsule overgrowth may be similar to the bands of inclusions observed in natural high-An feldspar, and we propose that in the natural phenocrysts, the bands of inclusions may be created by the

[1] Comprehensive mineral and glass composition data are on file at Oregon State Univ. and may be obtained from the authors.

formation of hopper crystals on pre-existing feldspars. Bands of inclusions formed in such a way would record the melt composition after the phenocryst had been undercooled, and not the composition and condition under which the phenocryst's core nucleated.

The question arises whether or not the cells, or inclusions, we observed were truly enclosed on all sides. It was not possible to answer this with certainty using two-dimensional imaging techniques, but several observations led us to conclude that most were likely enclosed. First, it was noted that when in inclusion bearing crystals from a single experiment were sectioned both along and across their long axes, the core was commonly enclosed on all sides in both orientations. Secondly, we limited the inclusions we analyzed to those with a more rounded appearance. Larger, more angular cells were considered to be possible open embayments and not true inclusions. Third, the average compositions of the inclusions were near-identical to the host glass, except for those formed during cooling. This is to be expected if the inclusions formed during cooling trapped liquids that were different from the composition at run temperature. In addition, although average compositions for inclusions formed during longer isothermal periods were similar to the host glass for each particular experiment, minor variability was present. This diversity may have resulted from entrapment of melt at an earlier stage in the experiment (Figure 9), as described in detail in the results. Such compositional differences between inclusions and inclusions and host glass, although small, would not be observed if the cells were open embayments.

The observation that cooling rate affected olivine morphology and inclusion frequency (the greatest frequency of olivine-hosted inclusions followed 10°/min. cooling) appears counterintuitive, since olivine did not crystallize until after 6 hours isothermal time, and olivine morphology would be not be expected to be influenced by cooling rate. However, Hort and Spohn (1991) have demonstrated that in small systems, thermal feedback from crystallization has the effect of extending the amounts of undercooling to small degree, and we suggest that thermal feedback from crystallizing feldspar produced an undercooling effect in the isothermal periods< 6 hours. The nucleation rate for plagioclase at the beginning of the isothermal period was dependent on the cooling rate (Table 2, Figure 4). As a result, the nucleation rate of plagioclase would control any thermal feedback, and thus the cooling rate could still influence the olivine morphologies that developed even after an isothermal interval.

Over longer isothermal times, the inclusion frequency could be affected by Ostwald ripening, an increase in grain size by dissolution of smaller crystals and a decrease in the number of crystals in a system at chemical equilibrium (Joesten, 1991, Park and Hanson, 1999; Baldan, 2002). This process results in smaller crystals with greater specific surface free energy dissolving and larger crystals increasing in size. The larger crystals must then be fewer in number due to mass balance constraints (Erbel, et al., 1998; Snyder, et al., 1999; Baldan, 2002). Ostwald ripening has long been recognized in both natural and synthetic materials as a control on the coarsening of a phase scattered in a homogeneous matrix of a second phase (Joesten, 1991; Baldan, 2002), and substantial coarsening of fosterite in haplobasaltic melts (SiO_2-Al_2O_3-CaO-MgO) has been attributed to Ostwald ripening (Park and Hanson, 1999). In our experiments, the system approached chemical equilibrium as the isothermal time progressed, which would favor possible Ostwald ripening. Although the number of crystals we observed did not follow any noticeable systematic variation with isothermal time, we did note some increase in grain size with run time, and very large olivine and plagioclase were observed in the 24 hour experiments and the116 hour experiment following 1°/min cooling. A complicating factor is the possibility that any temperature gradients, even small ones, in our system could cause additional mass transport that would obscure Ostwald ripening effects (Snyder, et al., 1999). Nevertheless, it must be considered that this process could have an influence on inclusion frequency in natural systems, and the longer a melt with phenocrysts remains at chemical equilibrium, the more likely coarsening and attendant decrease in the number of inclusions will take place. The possibility that Ostwald ripening could occur in crystallizing basaltic systems would have significant implications for olivine-hosted inclusions. Gaetani and Watson (2000, 2002) demonstrated that olivine-hosted inclusions might behave as open systems for major elements due to diffusive re-equilibration through the crystal lattice. If coarsening were to take place, the radii of smaller host crystals would decrease and that of larger crystals would increase over time. Because diffusive re-equilibration is controlled in part by the relative radii of inclusion and host crystal (Qin et al, 1992), the rate of inclusion modification then would not be constant in a system at chemical equilibrium, but instead would increase or decrease depending on whether the host crystal was dissolving and shrinking or growing larger.

Compositional Effects

Nearly all experimentally produced inclusions in olivine and plagioclase in a given experiment had average compositions near-identical to the surrounding glass. The experiments with inclusions formed only during cooling were exceptions, and these were not likely to be in equilibrium with the host glass at the quench time (Table 3 and 4, Figures 6-8). The lack of a systematic variation in composition with melt inclusion size (Figure 9) indicates that a boundary layer or diffusive profile was not entrapped during the formation of the melt inclusions in the experiments. Significantly, few inclusions formed during cooling and isothermal times of less than 6 hours following all cooling rates, and our results suggest that most inclusions formed with cooling followed by a short (at least 6 hours) isothermal period (Table 2). This indicates that the isothermal run times required for the formation of the majority of inclusions were long enough to limit the trapping of a boundary layer.

However, the diffusion coefficients in basalt for cations such as Ca, Na, Mg, and Fe^{2+} (Donaldson, 1975; Freer, 1981; Cooper et al., 1996) constrained cation transport in basalt liquid due to diffusion to 10^{-3}-10^{-7} μm/s at our run temperatures, slower than our estimated growth rates. In our small system with rapid cooling, it is possible that advective transport of cations aided in the dissipation of any boundary layer before the inclusions were sealed. Although growth in natural systems that produces incomplete morphologies with embayments and re-entrants would to also be more rapid than diffusion in the liquid, it is not during the development of the incomplete morphologies that inclusions are necessarily formed. Rather we suggest it is during the return to slower equilibrium growth that that the embayments are sealed off and the majority of inclusions formed, as planar growth occurs when the diffusion/growth rate approached unity (Lofgren, 1974). During this period of slower growth diffusion then would be able to dissipate a strong boundary layer.

In none of the experiments did we observe the formation of low-Ti inclusions in either olivine or plagioclase-hosted inclusions. For all inclusions and host glass, there was none of the K_2O diversity observed in natural melt inclusions, and K_2O contents are identical to the starting glass (Table 3 and 4). These data suggest that neither the low-Ti or variable K contents observed in natural MORB melt inclusions are the product of the entrapment process

Host glass compositions changed with increasing isothermal time, yet the average compositions of the melt inclusions remained within 2σ and analytical error to the host glass.

This seemingly presents a paradox, since we observed that in the case of experiments with 5º/min. cooling, the majority of inclusions formed between three and six hours isothermal time and one would expect to observe that inclusion compositions would remain similar to the 6-hour compositions in the 24 hour experiment. One likely explanation is that the EMP data were biased towards the last-formed inclusions, which would have similar compositions to the host glass at the time of quenching. The melt inclusion size distribution plots indicate that the size of the inclusions decreased with lengthening isothermal time (Figure 5) and the largest and most easily analyzed inclusions were likely those that formed closest to quench time. Also, our melt inclusion data sets for some experiments are small and may have missed the entire range of compositions. Figure 9 shows that while the mean compositions of melt inclusions from an individual experiment were similar to host glass there was some variability. Since this variability was not related to inclusion size, it is not considered a boundary effect. It is likely then that this diversity reflected melt trapped at earlier stages in the experiment when the evolving liquid had a different composition.

Implications for natural inclusions

We suggest that primary inclusions could form in a natural system that operates along time-temperature profiles similar to those of our experiments, although not at the rates and times we used. Such circumstances could occur in nature when a crystal bearing magma is rapidly cooled then allowed to thermally re-equilibrate. In one possible scenario, magma would ascend through a dike into cooler crust and undergo a moderate amount of cooling. This would then be followed by a short stagnation period before eruption. Under these conditions, cooling would take place much more rapidly than in the traditional magma body concept, e.g. ~0.1°/h in a dike compared to ~0.1°/yr in a magma chamber (Cooper et al., 2001). Although these cooling rates are slower than those used in our experiments, they do not preclude the development of the textures we observed, as skeletal and hopper crystals are observed in many dikes and sills (e.g. Ikeda, 1977, Philpotts, 1994, Hibbard, 1995, Cashman, 1993). Crystals may grow rapidly at rates of 10^{-6} cm/s or 10^{-2} μm/s (Ikeda, 1977; Cashman, 1993), comparable to growth rates in our experiments, with hopper/skeletal morphologies near the edge of a conduit. These crystals could later ascend into a larger upper magma body where growth rates would be several orders of magnitude slower (10^{-9} to 10^{-11} cm/s or 10^{-5} to 10^{-8} μm/s - Mangan, 1990; Cashman, 1993) and smooth, planar overgrowth would take place. In several igneous settings, this change from rapid crystal growth

with incomplete textures to slower crystal growth with smooth, planar surfaces and the consequent entrapment of melt might occur. For mid-ocean spreading centers it has been suggested that melt in the crust rises through a series of conduits (Sinton & Detrick, 1992; Kelemen et al., 1995) and collects in melt lenses (Kelemen et al., 1995; Garrido et al, 2001). In addition, crystals growing near the periphery of these bodies may cool much faster than in the center due to heat transport away from the sides of the melt lens by hydrothermal circulation (Phipps Morgan and Chen, 1993; Cherkaoui et al, 2003). Movement of the crystals to the center of the body would slow growth rate and result in the required change in morphology and entrapment of melt. For arc settings, models have been proposed in which melt propagates through fractures in the lithosphere and accumulates in the crust prior to eruption (Stern, 2002 and references therein). Similar rapid cooling and crystal growth followed by thermal re-equilibration with slower crystal growth could occur when a magma intrudes and mixes with a cooler magma. Crystals in the hotter magma would be subjected to undercooling that would produce more rapid growth and incomplete morphologies. As the intruding magma approached the temperature of the cooler magma, crystal growth would slow and consequent planar overgrowth would seal the embayments.

If entrapment does not lead to the diversity we observe in inclusions from natural phenocrysts, then such diversity indicates other processes at work. The host liquid composition may change over time with increasing crystallization and different periods of growth would entrap different liquids. In this case, inclusions should exhibit a spatial relationship between the location in the host and their composition. In circumstances involving the mixing of magmas with differing temperatures, some of the compositional diversity in natural inclusions could represent the effects of this mixing. Or more complex inclusion formation processes, including reaction and diffusion may be involved. In the cases of reaction and diffusion processes, inclusion compositional diversity should be more randomly distributed through the host crystal and there should be textural evidence (patchy zonation, sieve and fritted textures) for these processes. This reinforces the need for careful preliminary petrographic examination of the phenocrysts in a sample that will be separated for melt inclusion analysis. A combination of melt inclusion and CSD data could constrain the age of inclusions, and whether they formed before or after a change in crystallization conditions (Marsh, 1988; Roggensack, 2001). Melt

inclusion compositions should also be compared to the host lava composition to determine if the host could result form mixing of components with the compositions of the inclusions.

CONCLUSIONS

The results of our experiments show that melt inclusions in high-An plagioclase and high-Fo olivine in low pressure, anhydrous mafic melts can arise from changes in growth mechanisms and crystal morphology due to undercooling and subsequent isothermal crystallization. Hopper and skeletal crystals occur when a combination of undercooling and cooling promotes growth controlled by dissipation of heat and impurities during undercooling. For our system, cooling rates of 5°/min. for plagioclase and 10°/min. for olivine were the most favorable for the formation of hopper crystals. A subsequent period of isothermal crystallization will result in a change in the rate-limiting step in crystal from heat/impurity dissipation-controlled growth to surface nucleation and diffusion-controlled growth. The result of this change in dominant growth mechanism is planar overgrowth on the hopper and skeletal crystals and the entrapment of melt. Since this is the dominant inclusion formation mechanism, most of the experimentally produced inclusions form during isothermal crystallization following cooling.

The experiments with 6-hour and greater isothermal periods exhibited the highest frequencies of inclusions, and these times appear sufficiently long to preclude trapping a boundary layer or diffusive profile. For this reason, all experimentally produced inclusions in olivine and plagioclase have compositions identical to the surrounding glass, except in the case of the few inclusions formed during cooling. With a long isothermal period (1l6 hours), the frequency of inclusions decreased (Table 2) and the size of crystals increased. This may indicate that coarsening processes, such as Ostwald ripening occur during longer isothermal periods and such processes may reduce the number of inclusions over time. The implication of this is that longer crystal residence times could potentially eliminate most inclusions and thus MI compositions would record only short periods in a magma's evolution. Circumstances in nature similar to our experimental conditions may occur when a partial melt rises through a conduit into cooler crust and stagnates at low pressure (<10 kb) prior to eruption and quenching, or when magmas of differing temperatures mix.

While our suggested mechanism may be valid for primary inclusions, it does not remove secondary inclusion formation and diffusional processes from consideration when dealing with natural samples. It is important to note that negative crystal shape alone (i.e. re-entrants and

cellular texture) is not proof of primary origin (Roedder, 1984). This reinforces the need for careful preliminary petrographic examination of phases that will be separated for melt inclusion analyses.

Acknowledgements

We wish to thank L. Danyushevsky for his helpful comments and suggestions, and an anonymous reviewer for their concerns and the very useful suggestion to compare inclusion sizes and compositions. This work was funded by NSF grant EAR 9903137.

REFERENCES

Anderson, A T, (1974) Evidence for a picritic volatile-rich magma beneath Mt. Shasta, California, J. Petrol. 15: 243-267

Anderson, A T and Wright, T L (1972) Phenocrysts and glass inclusions and their bearing on oxidation and mixing of basaltic magmas, Kilauea volcano, Hawaii, Am. Mineral. 57: 188-216

Baldan, A (2002) Progress in Ostwald ripening theories and their applications to nickel-base superalloys J. Mater. Sci. 37:2171-2202

Bodnar, R J and Sterner, S M (1984) Synthesis of fluid inclusions in natural quartz, Eos Trans., 78:

Cashman, K V (1988) Crystallization of Mount St. Helens 1980-1986 dacite: a quantitative textural approach, Bull. Volcanol. 50: 194-209

Cashman, K V (1993) Relationship between plagioclase crystallization and cooling rate in basaltic melts, Contrib. Mineral. Petrol. 113: 126-142

Cashman, K V and Ferry, J M (1988) Crystal size distribution (CSD) in rocks and the kinetics and dynamics of crystallization III. Metamorphic crystallization, Contrib. Mineral. Petrol. 99: 401-415

Cashman, K V and Marsh, B D (1984) Crystal-size spectra and kinetics of crystal growth in magmas II. Application. Geol. Soc. Am. Abstr. Programs, 16: 465

Cherkaoui, A S M, Wilcock, W S D, Dunn, R A, Toomey, D R, (2003) A numerical model of hydrothermal cooling and crustal accretion at a fast spreading mid-ocean ridge Geochem. Geophys. Geosys. 4: doi:10.1029/2001GC000215

Corrigan, G M (1982) The crystal morphology of plagioclase feldspar produced during isothermal supercooling and constant rate cooling experiments, Miner. Mag. 46: 433-439.

Cooper, K M, Reid, M R, Murell, M T, Clague, D A (2001) Crystal and magma residence at Kilauea Volcano, Hawaii: 230^{Th}-226^{Ra} dating of the 1955 east rift eruption, Earth Planet. Sci. Lett. 184: 703-718.

Danyushevsky, L V, McNeill, A W, and Sobolev, A V (2002) Experimental and petrological studies of melt inclusions in phenocrysts from mantle-derived magmas: an overview of techniques, advantages and complications, Chem. Geol. 183: 5-24

Davis, A S and Clague, D A (1987) Geochemistry, mineralogy, and petrogenesis of basalt from the Gorda Ridge, J. Geophys. Res. 92: 10467-10483

Donaldson, C H (1975) Calculated diffusion coefficients and the growth rate of olivine in a basalt magma, Lithos 8: 163-174

Donaldson, C H (1976) An experimental investigation of olivine morphology, Contrib. Mineral. Petrol. 57: 187-213

Erbel, DD, Drits, VA, and Środoń, J (1998) Deducing growth mechanisms for minerals from the shapes of crystal size distributions Am. J. Sci. 298:499-533

Faure, F, Trolliard, G, Nicollet, C, Montel, J-M (2003) A developmental model of olivine morphology as a function of the cooling rate and the degree of undercooling, Contrib. Mineral. Petrol. 145: 251-263

Freer, R (1981) Diffusion in silicate minerals and glasses: a data digest and guide to the literature, Contrib. Mineral. Petrol. 76: 440-454

Gaetani, G A and Watson, E B (2000) Open system behavior of olivine-hosted melt inclusions, Earth Planet. Sci. Lett. 183: 27-41

Gaetani, G A and Watson, E B (2002) Modeling the major-element evolution of olivine-hosted melt inclusions, Chem. Geol. 183: 25-41

Garrido, C J, Kelemen, P B, and Hirth, G (2001) Variation of cooling rate with depth in lower crust formed at an oceanic spreading ridge: plagioclase size distributions in gabbros from the Oman ophiolite, Geochem, Geophys, Geosyst. 2 doi:10.1029/2000GC000136

Hibbard, M J (1995) Petrography to petrogenesis, Prentice Hall, Englewood Cliffs, NJ 587p

Higgins, M D (2000) Measurement of crystal size distributions Am. Mineral. 85: 1105-1116

Hort, M and Spohn, T (1991) Crystallization calculations for a binary melt cooling at constant rates of heat removal, implications for the crystallization of magma bodies, Earth Planet. Sci. Lett. 107: 463-474.

Ikeda, Y (1977) Grain size of plagioclase of the basaltic andesite dikes, Iritono, central Abukuma plateau, Can. J. Earth Sci. 14: 1860-1866.

Jambon, A, Lussiez, P, Clocchiatti, R, (1992) Olivine growth rates in a tholeiitic basalt; an experimental study of melt inclusions in plagioclase, Chem. Geol. 96: 277-287

Joesten, RL (1991) Kinetics of coarsening and diffusion-controlled mineral growth. In: Kerrick, DM (ed) Contact metamorphism. Reviews in mineralogy, vol. 26, Mineral. Soc. Am.: 507-582.

Johnson, J, Nielsen, R L, and Fisk, M R, (1996) Plagioclase-hosted melt inclusions in the Steens Mountain Basalts, Southeastern Oregon, Petrol. 4: 267-273

Kelemen, P B, Shimizu, N and Salters, V J M (1995) Extraction of mid-ocean ridge basalt from the upwelling mantle by focused flow of melt in dunite channels, Nature, 375: 747–753

Kohut, E J and Nielsen, R L (2003) Low pressure phase equilibria of anhydrous anorthite-bearing mafic magmas, Geochem. Geophys. Geosyst. Doi: 10.1029/2002GC000451

Lofgren, G (1974) An experimental study of plagioclase crystal morphology: Isothermal crystallization Am. J. Sci. 274: 243-273

Marsh, B D (1984) Crystal-size spectra and kinetics of crystal growth in magma: I. Theory Geol. Soc. Am., Abstr. Programs 16: 585

Marsh, B D (1988) Crystal size distributions (CSD) in rocks and the kinetics and dynamics of crystallization I. Theory Contrib. Mineral. Petrol. 99: 277-291

Mangan, M T (1990) Crystal size distribution systematics and the determination of magma storage times: the 1959 eruption of Kilauea volcano, Hawaii J. Volc. Geotherm. Res. 44: 295-302

McNeill, A W and Danyushevsky, L V (1996) Compositions and crystallization temperatures of primary melts for hole 896A basalts: evidence from melt inclusion studies, Proc. ODP, Scientific results, 148: 21-35

Michael, P J, McDonough, W F, Nielsen, R L, Cornell, W C (2002) Depleted melt inclusions in MORB plagioclase; messages from the mantle or mirages in the magma chamber? Chem. Geol. 183: 43-61

Mueller, R F and Saxena, S K (1977) Chemical petrology with applications to the terrestrial planets and meteorites, Springer-Verlag, New York, 394 p.

Muncill, GE and Lasaga, AC (1987) Crystal-growth kinetics of plagioclase in igneous systems: one-atmosphere experiments and application of a simplified growth model, Am. Mineral. 72: 299-311

Muncill, GE and Lasaga, AC (1988) Crystal-growth kinetics of plagioclase in igneous systems: Isothermal H_2O-saturated experiments and extension of a growth model to complex silicate melts, Am. Mineral. 73: 982-992

Nakamura and Shimikita, (1998) Dissolution origin and syn-entrapment compositional change of melt inclusion in plagioclase, Earth Planet. Sci. Lett.161: 119-133

Nielsen, R L, Crum, J, Bourgeois, R, Hascall, K, Forsythe, L M, Fisk, M R, Christie, D M (1995) Melt inclusions in high-An plagioclase from the Gorda Ridge, an example of the local diversity of MORB parent magmas, Contrib. Mineral. Petrol. 122: 34-50

Osborn, E F and Tait, D B (1952) The system diopside-anorthite-forsterite Amer. J. Science Bowen Volume: 413-433

Panjasawatwong, Y, Danyushevsky, L V, Crawford, A J, Harris, K L (1995) An experimental study of the effects of melt composition on plagioclase-melt equilibria at 5 and 10 kbar:

implications for the origin of high-An plagioclase in arc and MORB magmas, Contrib. Mineral. Petrol. 18: 420-435

Park, Y and Hanson, B (1999) Experimental investigation of Ostwald-ripening rates of forsterite in the haploblastic system, J Volcan. Geotherm. Res. 90: 103-113.

Philpotts, A R (1994) Principles of igneous and metamorphic petrology, Prentice Hall, Englewood Cliffs, NJ pp. 215-234

Phipps Morgan, J., and Y. J. Chen (1993) The genesis of oceanic crust: Magma injection, hydrothermal circulation, and crustal flow, J. Geophys. Res. 98: 6283–6297

Qin, Z, Lu, F, Anderson, A T (1992) Diffusive reequilibration of melt and fluid inclusions, Am. Mineral. 77: 565-576

Roedder, E (1984) Fluid inclusions: Ribbe, P H (ed) Reviews in Mineralogy, vol. 12. Mineralogical Society of America, Blacksburg, VA, 646p

Roggensack, K (2001) Sizing up crystals and their melt inclusions: a new approach to crystallization studies, Earth Planet. Sci. Lett. 187: 221-237

Saal, A E, Hart, S R, Shimizu, N, Hauri, E H, Layne, G D, (1998) Pb isotopic variability in melt inclusions from oceanic island basalts, Polynesia, Science, 282: 1481-1484

Sinton, C W, Christie, D M, Coombs, V L, Nielsen, R L, Fisk, M R (1993) Near-primary melt inclusions in anorthite phenocrysts from the Galapagos Platform, Earth Planet. Sci. Lett. 119: 527-537

Sinton, J M and Detrick, R S (1992) Mid-ocean ridge magma chambers, J. Geophys. Res. 97: 197–216

Sisson, T W and Bronto, S (1998) Evidence for pressure-release melting beneath magmatic arcs from basalt at Galunggung, Indonesia, Nature, 391: 883-886

Snyder, VA, Akaiwa, N, Alkemper, J, and Vorrhees, PW (1999) The influence of temperature gradients on Ostwald Ripening, Metal. Mater. Trans. A., 30A: 2341-2348

Sobolev, A V (1996) Melt inclusions in minerals as a source of petrological information, Petrology, 4: 228-239

Sobolev, A V and Shimizu, N, (1993) Ultra-depleted primary melt included in an olivine from the Mid- Atlantic Ridge, Nature, 363: 151-154

Sours-Page, R, Johnson, K T M, Nielsen, R L, Karsten, J L (1999) Local and regional variation of MORB parent magmas: evidence from melt inclusions from the Endeavour segment of the Juan de Fuca Ridge, Contrib. Mineral. Petrol. 134: 342-363

Sours-Page, R, Nielsen, R L, Batiza, R, (2002) Melt inclusions as indicators of parental magma diversity on the northern East Pacific Rise, Chem. Geol., 183: 237-261

Stern, R J (2002) Subduction zones, Rev. Geophys. Doi:10.1029/2001RG000108

Student, J J and Bodnar, R J (1996) Melt inclusion microthermometry: petrologic constraints from the H_2O saturated haplogranite system, Petrology, 4: 291-306

Student, J J and Bodnar, R J (1997) Modeling the P-V-T-X properties of haplogranite melt inclusions during heating and cooling, Eos Trans., 78: S0429

Student, J J and Bodnar, R J (1999) Synthetic fluid inclusions XIV: microthermometric and compositional analysis of coexisting silicate melt and aqueous fluid trapped in the haplogranite-H_2O-NaCl-KCl system at 800º C and 2000 bars, J. Petrol., 40: 1509-1525

Watson E B (1976) Glass inclusions as samples of early magmatic liquid: determinative method and application to a South Atlantic basalt, J. Volcanol. Geotherm. Res. 148: 527-544

FIGURES

Fig 1 Drawings based on backscattered electron images for representative plagioclase morphologies. A-swallowtail, B-skeletal, C-simple hopper growing from skeletal crystal, D-blocky hopper with inclusions, E- tabular crystal with inclusions. See text for explanation.

Fig 2 (a. top) Backscattered electron image of granular olivine with central inclusion (arrow). **(b. bottom)** Backscattered electron image of a wide variety of olivine (dark gray) hopper crystals in the quenched run products from experiment with 1º/min. cooling to 1230º C (70º ΔT) and 6 hours isothermal period. Light gray crystals are plagioclase (Pl) and small white rounded objects are chromites. Note that several olivines host inclusions (arrows).

Fig 3 (a. top) Backscattered electron image of plagioclase (Pl) hoppers in the quenched run products from an experiment with 5º/min. cooling to 1230º C (70º ΔT) and 6 hours isothermal period. Hoppers occurred both as free-floating crystals in the liquid and as overgrowth on the anorthite capsule rim. Note band of inclusions (arrows) in rim overgrowth. Growth of similar hoppers on natural feldspars may form the bands of inclusions observed in many plagioclase phenocrysts **(b. bottom)** Backscattered electron image of tabular plagioclase (Pl) containing melt inclusions (arrows). Experiment cooled at 10º /min to 70º ΔT (1230º C), held for 24 hours and quenched. We propose that such crystals initially developed hopper and skeletal morphologies during undercooling and isothermal crystallization of 6 hours or less. Growth became planar as isothermal crystallization progressed, and planar overgrowth trapped melt in embayments in the initial hopper and skeletal morphologies.

Fig 4 Representative growth and nucleation rates for experiments with 70°ΔT calculated using CSD methods. Run times are the sum of cooling and isothermal times. G was fastest during cooling and decreased with lengthening isothermal period. G and J were highest during 10º /min. cooling. The decrease in G and J coincided with the change to more complete crystal morphologies with smooth, planar faces.

Fig 5 Representative melt inclusion size distributions for experiments with 1º/min. cooling to 70º ΔT. Size distribution curves remained fairly constant and weighted towards smaller inclusion sizes, especially for the 116-hour experiment.

Fig 6 Variation diagram for major elements vs. MgO for representative experiments with 70º ΔT, and 1º/min. cooling. Points are average compositions. Davis and Clague refers to the lava suite from which the starting glass was sampled (D9-2 Davis and Clague, 1987). Error range includes 2σ from average (Table 4) and analytical error (see text).

Fig 7 Variation diagram for major elements vs. MgO for experiments with 70º ΔT, and 5º/min. cooling.

Fig 8 Variation diagram for major elements vs. MgO for experiments with 70º ΔT, and 10º/min. cooling.

Fig 9 Inclusion size vs. representative compositions. Compositions chosen to represent cations rejected during growth that may be present in a boundary layer surrounding the crystal. CaO and Al_2O_3 are shown for olivine-hosted inclusions (a), Mg# and TiO_2 for plagioclase-hosted inclusions (b). Note that there was no systematic variation with size, indicating that an entrapped boundary layer was not detected. Variation that was present may reflect melt trapped at different points in the experiment run time.

Fig 10 Predicted and observed An contents for feldspars vs. isothermal crystallization time. For unzoned feldspars, An numbers refer to averages for whole crystals. Errors are standard deviation from average. Predicted An Pan. points are expected An values calculated using Panasawatwong et al. (1995) equation 1, Predicted An Dan. are predicted An values using Danyushevsky's model in Petrolog software. Note feldspar compositions approached predicted equilibrium values with increasing isothermal time, which correlates with the change to more equilibrium, planar crystal morphologies.

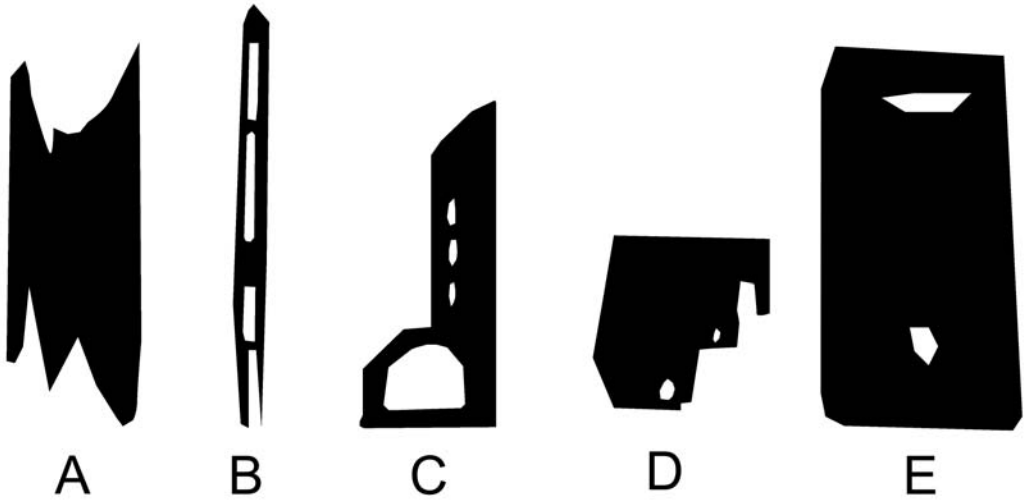

Figure 1

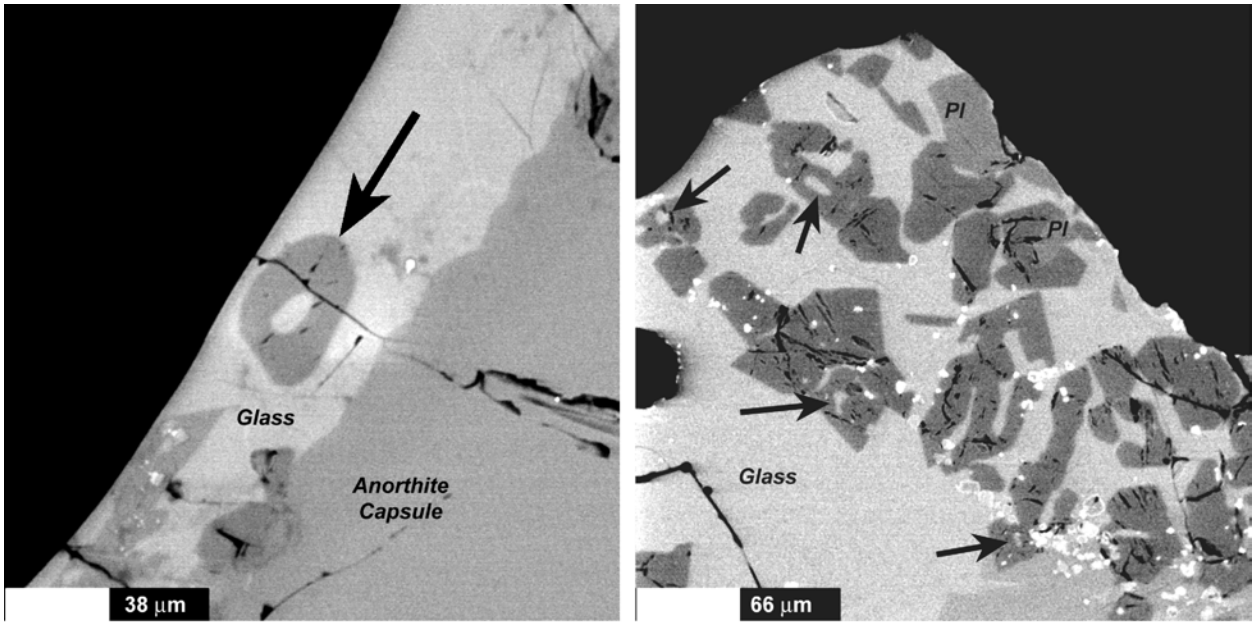

Figure 2

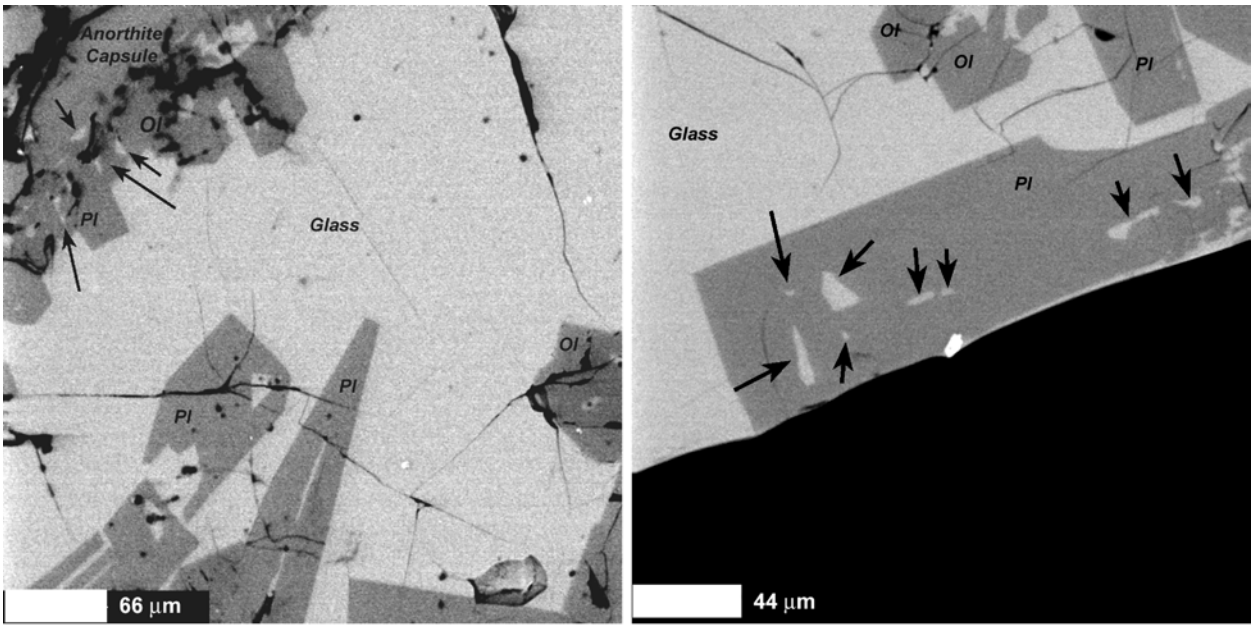
Anorthite
Capsule
Ol
Pl
Glass
Ol
Pl
Pl
66 μm
Ol
Ol
Pl
Glass
Pl
44 μm

a. b.

Figure 3

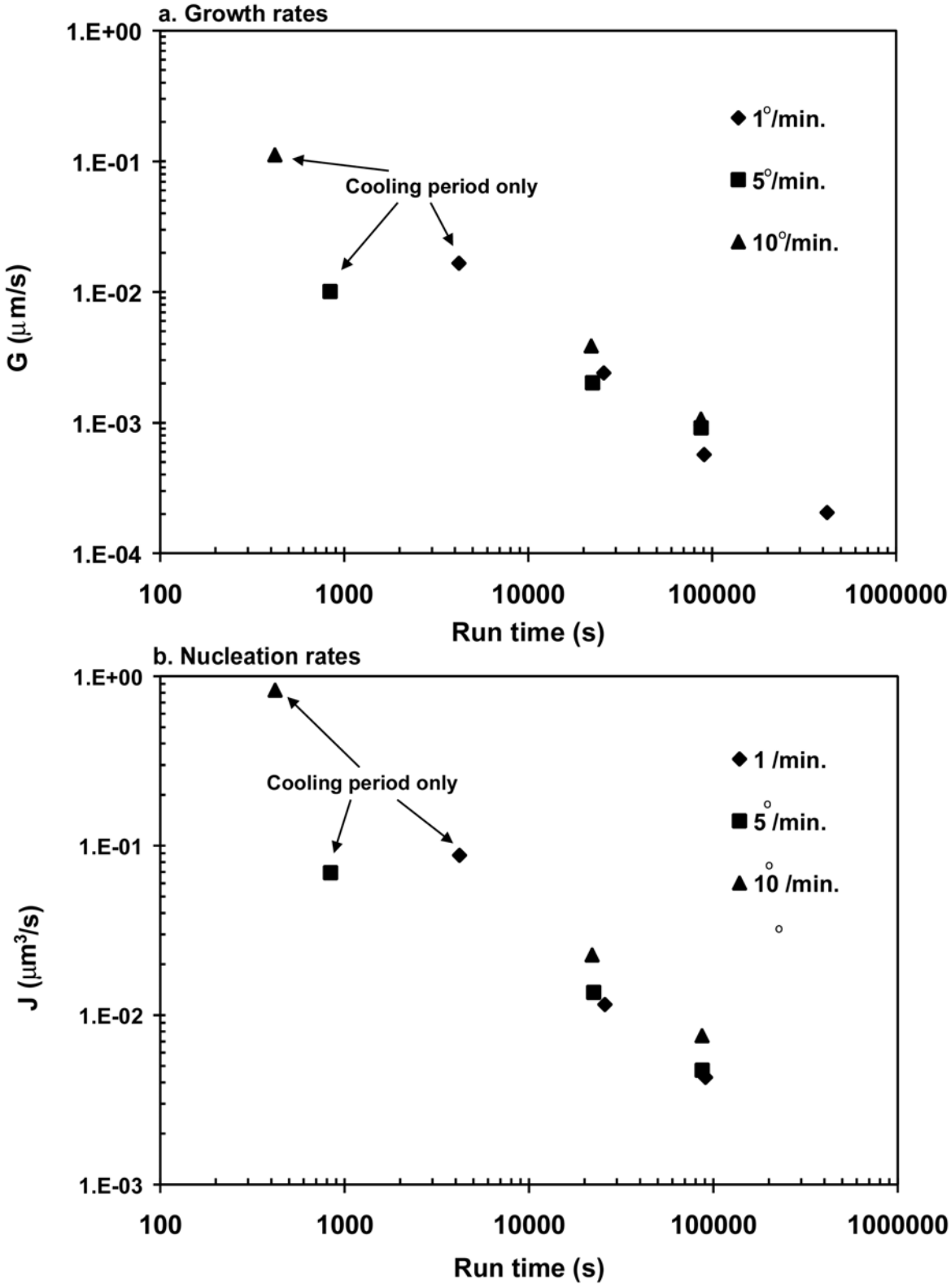
a. Growth rates
1.E+00
1.E-01
1.E-02
1.E-03
1.E-04
G (μm/s)
Cooling period only
1°/min.
5°/min.
10°/min.
100
1000
10000
100000
1000000
Run time (s)
b. Nucleation rates
1.E+00
1.E-01
1.E-02
1.E-03
J (μm³/s)
Cooling period only
1 /min.
5 /min.
10 /min.
100
1000
10000
100000
1000000
Run time (s)

Figure 4

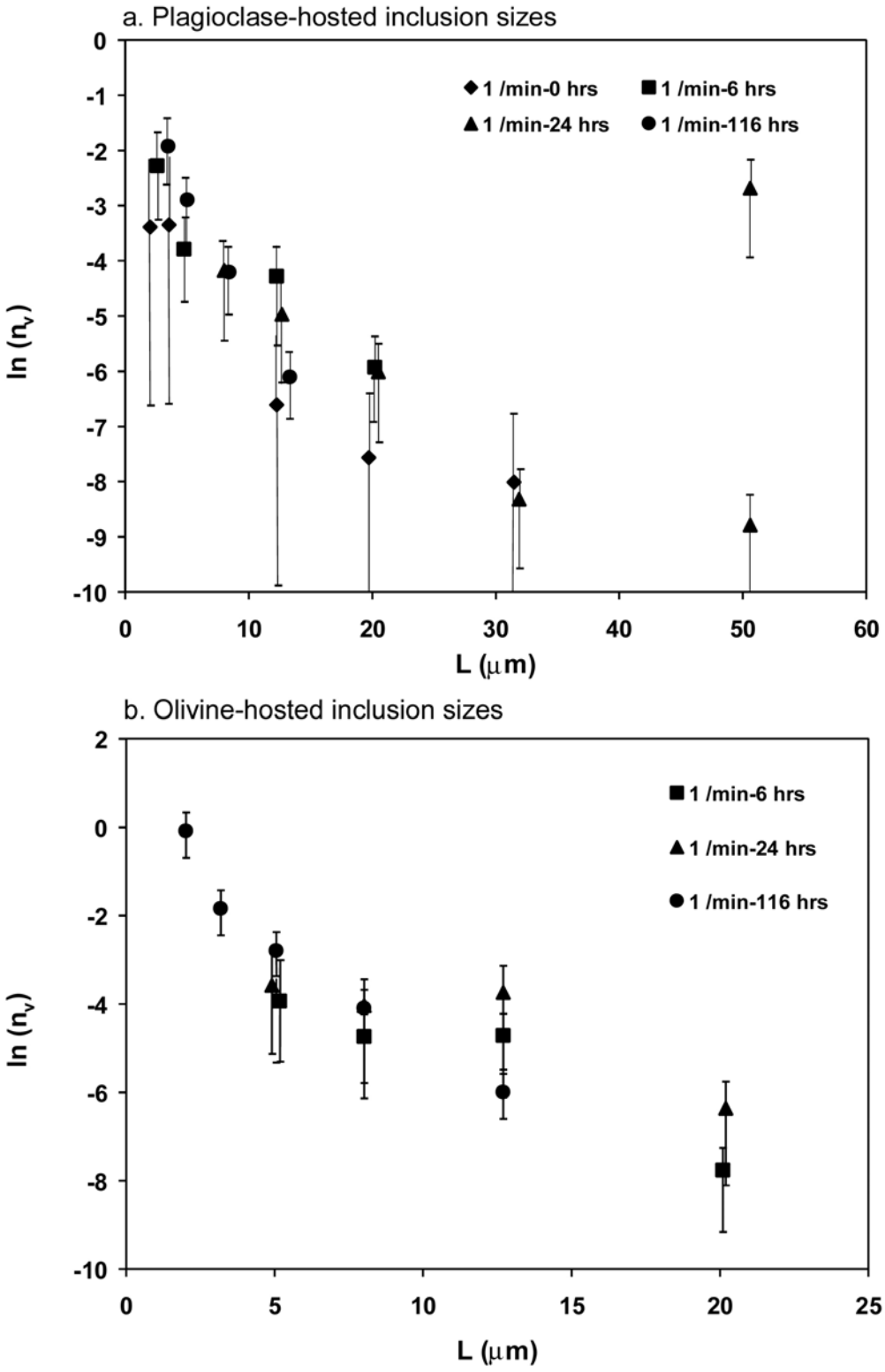
a. Plagioclase-hosted inclusion sizes
1 /min-0 hrs
1 /min-6 hrs
1 /min-24 hrs
1 /min-116 hrs
ln (nv)
L (μm)
b. Olivine-hosted inclusion sizes
1 /min-6 hrs
1 /min-24 hrs
1 /min-116 hrs
ln (nv)
L (μm)

Figure 5

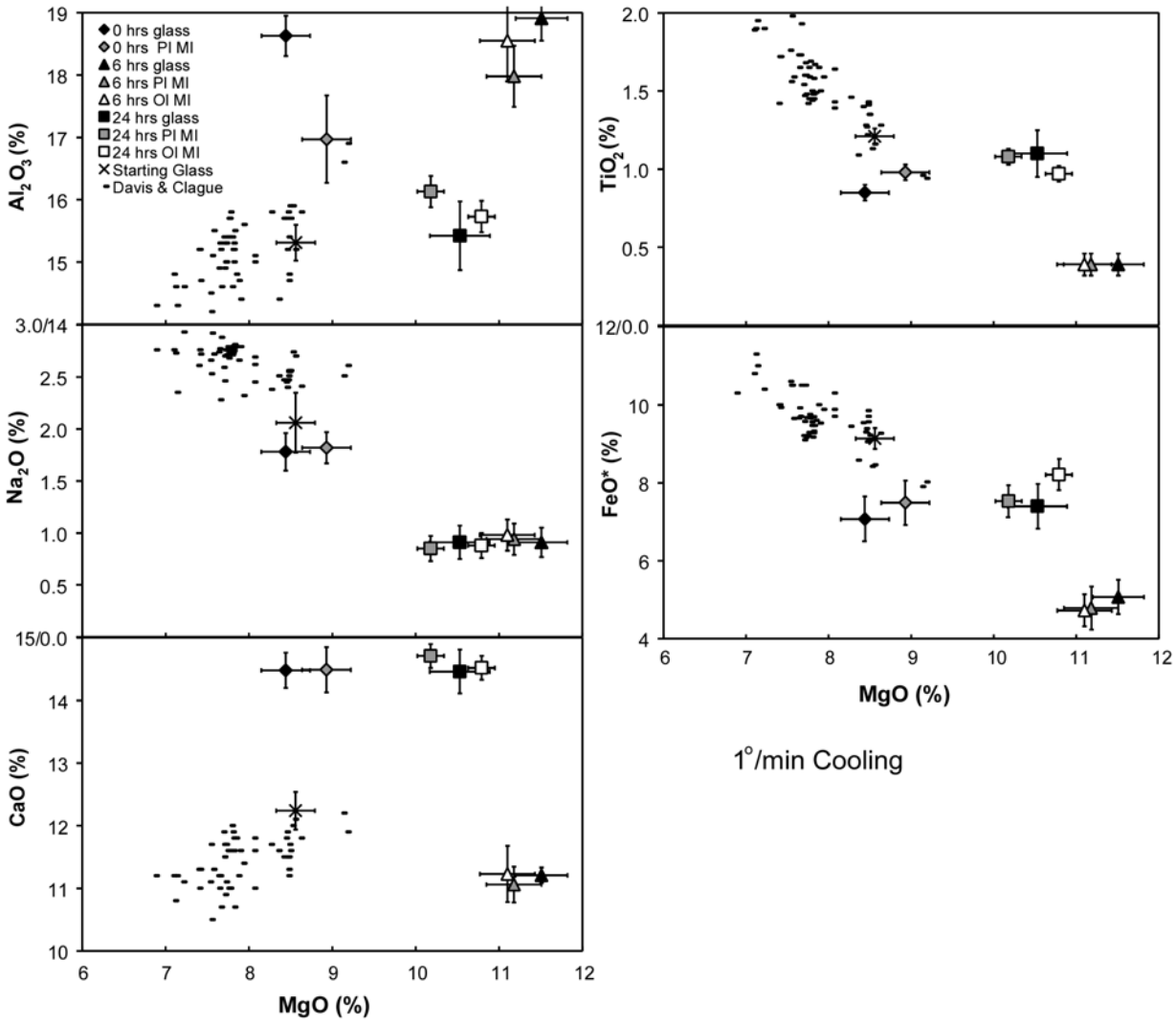
0 hrs glass
0 hrs Pl MI
6 hrs glass
6 hrs Pl MI
6 hrs Ol MI
24 hrs glass
24 hrs Pl MI
24 hrs Ol MI
Starting Glass
Davis & Clague
Al2O3 (%)
Na2O (%)
CaO (%)
TiO2 (%)
FeO* (%)
MgO (%)
MgO (%)
1°/min Cooling

Figure 6

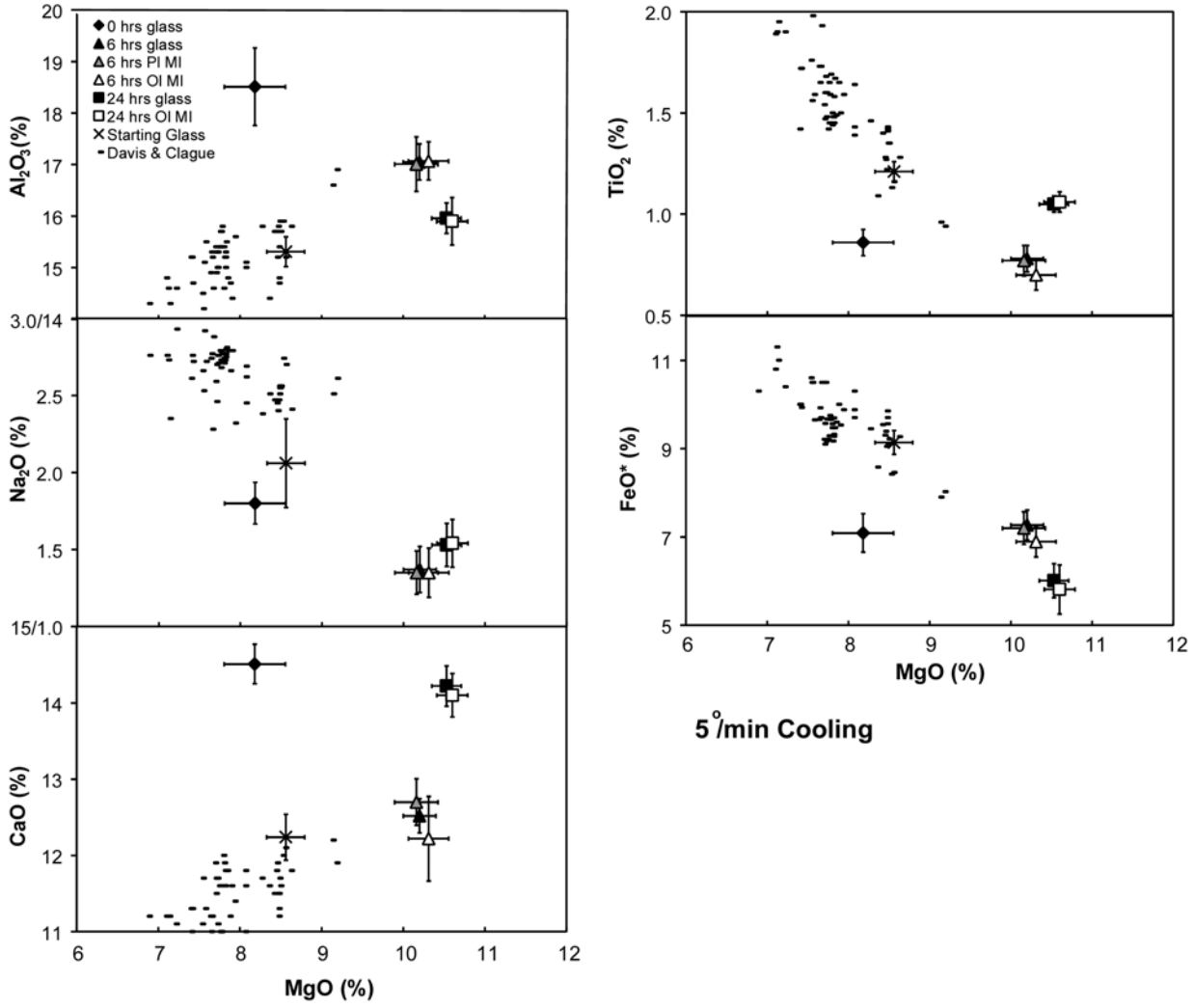
0 hrs glass
6 hrs glass
6 hrs Pl MI
6 hrs Ol MI
24 hrs glass
24 hrs Ol MI
Starting Glass
Davis & Clague
Al2O3 (%)
Na2O (%)
CaO (%)
TiO2 (%)
FeO* (%)
MgO (%)
5°/min Cooling

Figure 7

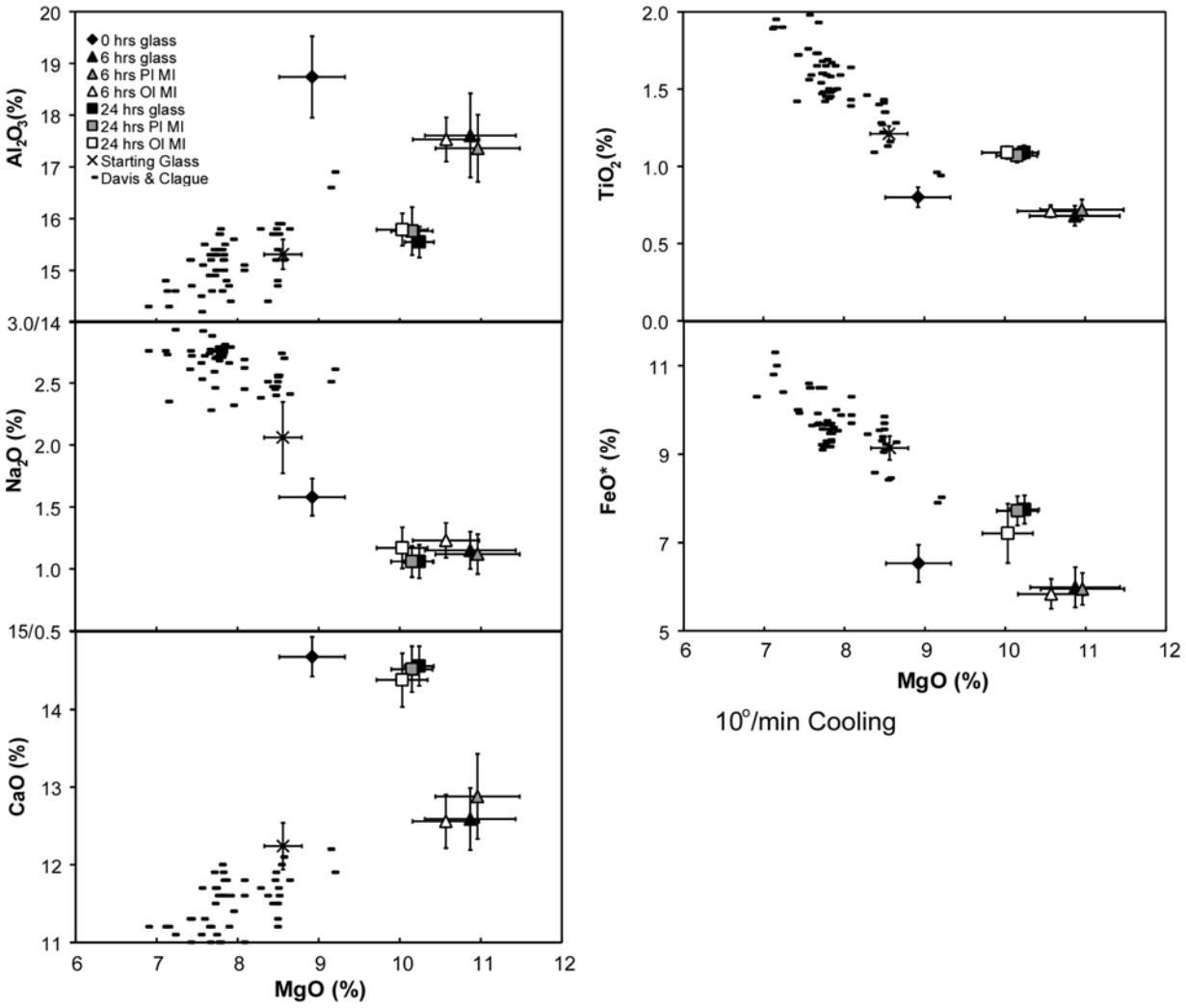
0 hrs glass
6 hrs glass
6 hrs Pl MI
6 hrs Ol MI
24 hrs glass
24 hrs Pl MI
24 hrs Ol MI
Starting Glass
Davis & Clague
Al2O3(%)
Na2O (%)
CaO (%)
TiO2 (%)
FeO* (%)
MgO (%)
10°/min Cooling

Figure 8

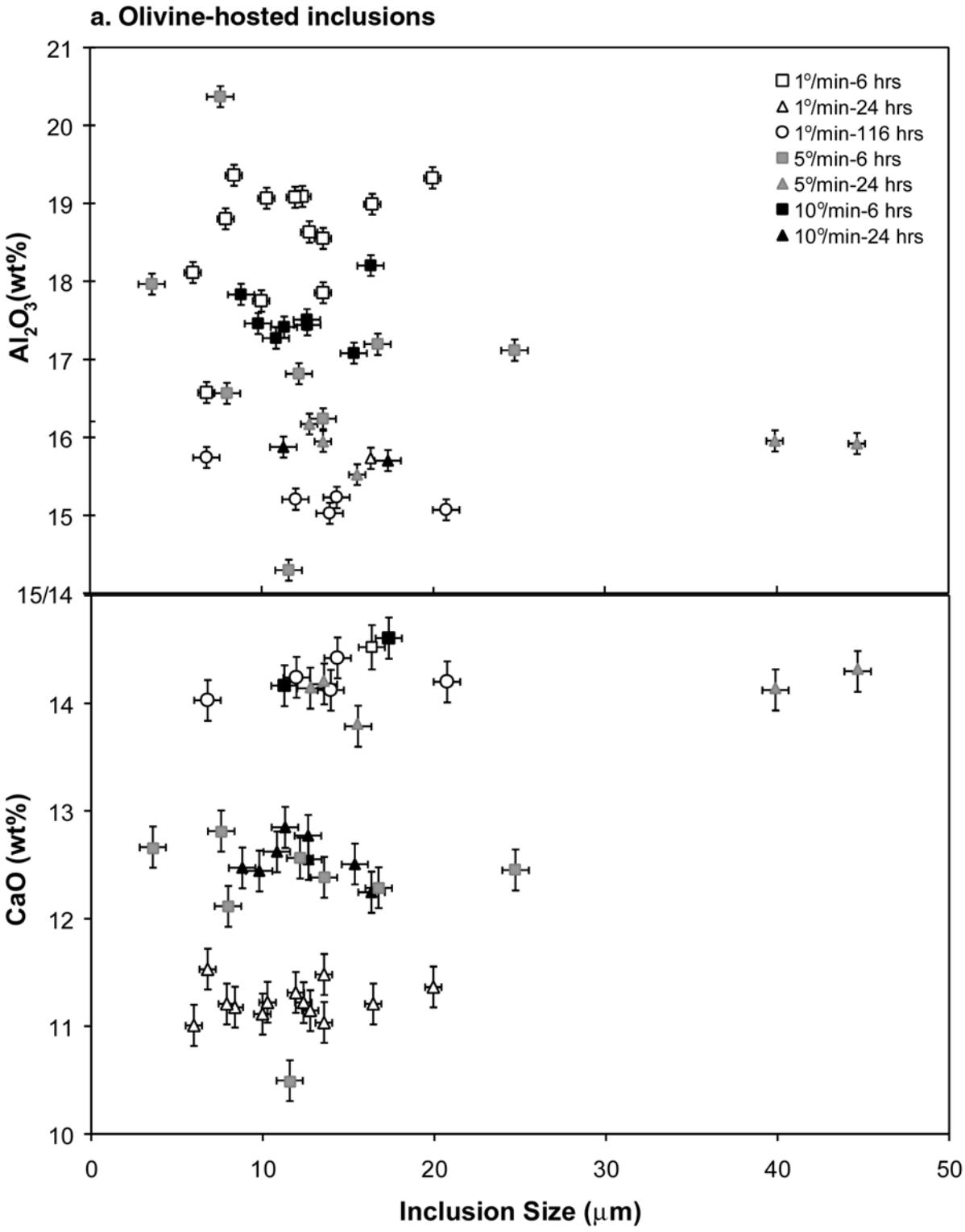
a. Olivine-hosted inclusions
1°/min-6 hrs
1°/min-24 hrs
1°/min-116 hrs
5°/min-6 hrs
5°/min-24 hrs
10°/min-6 hrs
10°/min-24 hrs
Al2O3(wt%)
CaO (wt%)
Inclusion Size (μm)
21
20
19
18
17
16
15
15/14
14
13
12
11
10
0
10
20
30
40
50

Figure 9a.

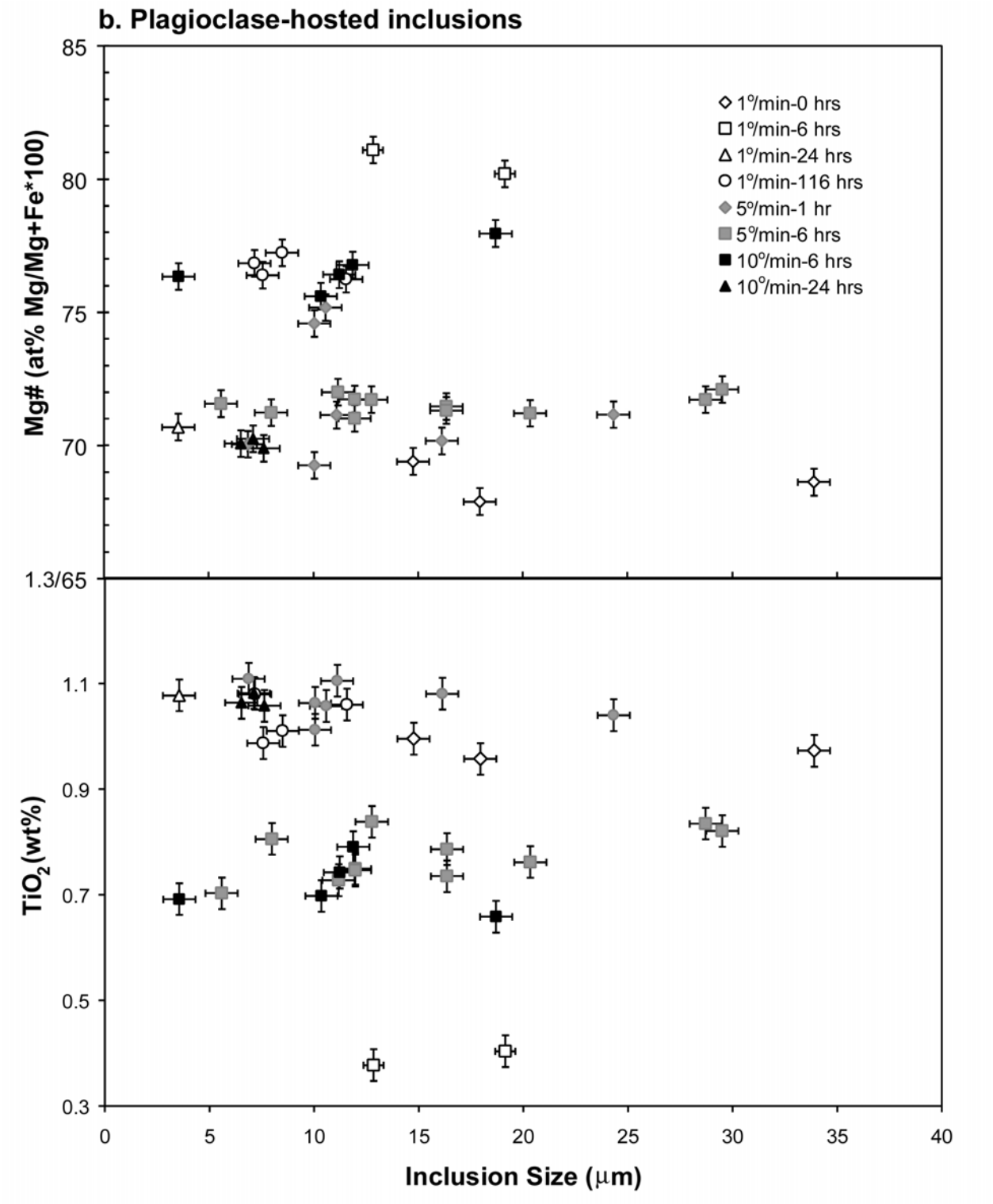
b. Plagioclase-hosted inclusions
Mg# (at% Mg/Mg+Fe*100)
85
80
75
70
1.3/65
1°/min-0 hrs
1°/min-6 hrs
1°/min-24 hrs
1°/min-116 hrs
5°/min-1 hr
5°/min-6 hrs
10°/min-6 hrs
10°/min-24 hrs
TiO2 (wt%)
1.1
0.9
0.7
0.5
0.3
0
5
10
15
20
25
30
35
40
Inclusion Size (μm)

Figure 9b

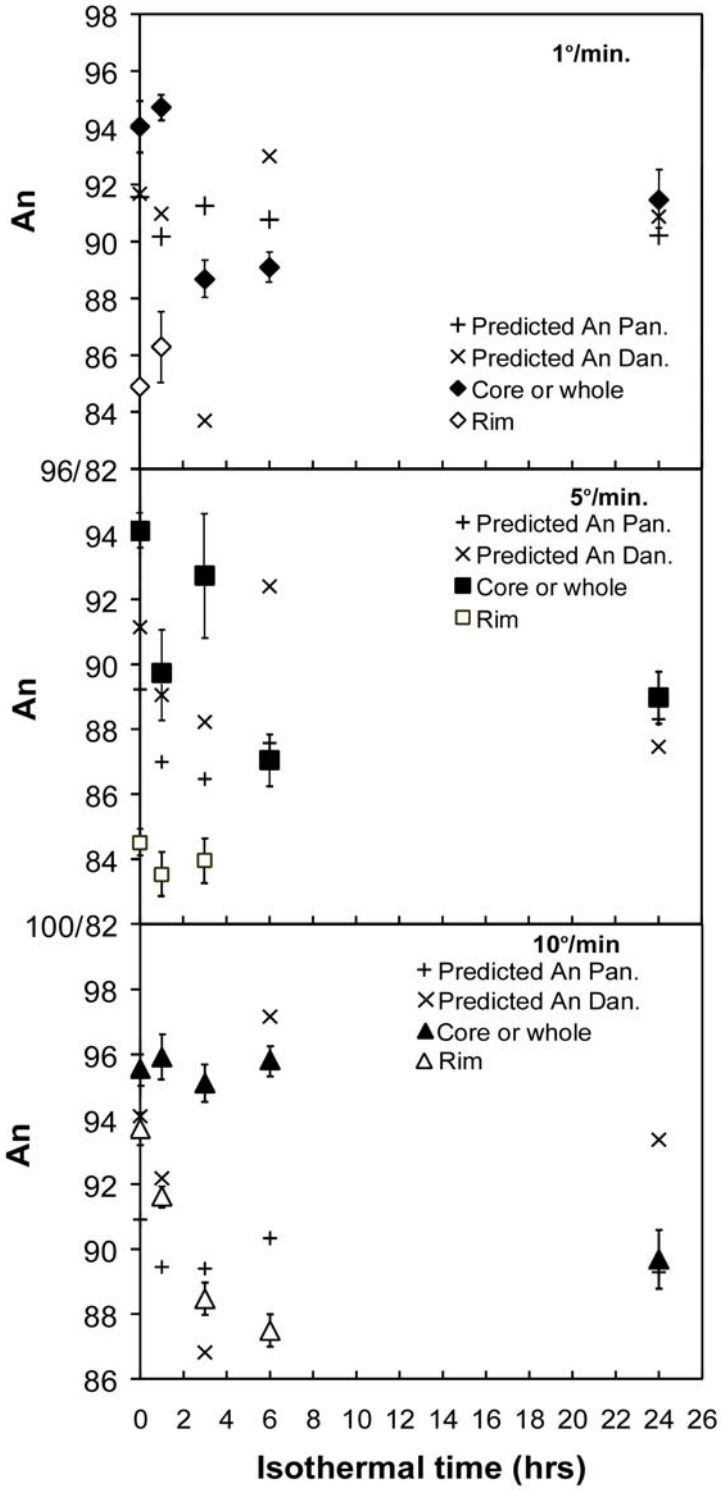
1°/min.
+ Predicted An Pan.
× Predicted An Dan.
◆ Core or whole
◇ Rim
5°/min.
+ Predicted An Pan.
× Predicted An Dan.
■ Core or whole
□ Rim
10°/min
+ Predicted An Pan.
× Predicted An Dan.
▲ Core or whole
△ Rim
An
Isothermal time (hrs)

Figure 10

TABLES

Table 1: Morphologies of plagioclase and olivine in the run products as functions of undercooling, cooling rate, and isothermal run time.

Table 2: Plagioclase and olivine growth rates and inclusion frequencies.

Table 3: Compositions of host glass and melt inclusions for experiments run at 90º ΔT determined by WDS analyses using the electron microprobe.

Table 4: Compositions of host glass and melt inclusions for experiments run at 70º ΔT determined by WDS analyses using the electron microprobe.

Table 5: Summary of mineral compositions determined by WDS analyses using the electron microprobe. Where no An value for rim is listed, most feldspars were not zoned and An value for core refers to average An value for whole crystals.

Table 1. Plagioclase Morphology

$\Delta T=90^o$			
Run Time (hrs)	1^o/min.	5^o/min.	10^o/min.
0	skeletal/complex swallowtail	simple swallowtail/tabular*	tabular-equant*
6	blocky hopper	skeletal	tabular/hopper
$\Delta T=70^o$			
Run Time (hrs)	1^o/min.	5^o/min.	10^o/min.
0	simple swallowtail	skeletal/tabular	tabular/swallowtail
1	swallowtail/skeletal	skeletal	tabular/swallowtail
3	skeletal	skeletal/hopper	swallowtail/skeletal
6	skeletal/blocky hopper	complex hopper/skeletal	blocky/complex hopper
24	complex hopper/tabular*	tabular-equant*	blocky hopper
116	tabular-equant*/hopper	-	-

Olivine Morphology

$\Delta T=90^o$			
Run Time (hrs)	1^o/min.	5^o/min.	10^o/min.
0	no olivine	no olivine	no olivine
6	simple, C-hopper	hook-hopper	intergrown
$\Delta T=70^o$			
Run Time (hrs)	1^o/min.	5^o/min.	10^o/min.
0	no olivine	no olivine	no olivine
1	no olivine	no olivine	no olivine
3	no olivine	no olivine	hook, C-hopper/granular
6	granular/hopper	granular	granular/hook-hopper
24	intergrown/polyhedral***	hook and complex hopper	simple hopper/polyhedral*
116	polyhedral/simple hopper	-	-

*crystals have incipient hopper features
**tabular and/or equant crystals hosting inclusions
***inclusion hosting

Table 2: Growth rates and melt inclusion frequencies

ΔT	Cooling rate	Isothermal time	Plag. G	Plag. J	Olivine G	# Pl MI / # Pl Xtals	# Ol MI / # Ol Xtals
90°	1	0	1.02×10^{-2}	3.33×10^{-2}	-	0.136	-
90°	5	0	1.09×10^{-3}	4.37×10^{-2}	-	0.235	-
90°	10	0	1.12×10^{-3}	9.11×10^{-2}	-	-	-
90°	1	6	8.80×10^{-4}	7.11×10^{-3}	1.25×10^{-3}	0.462	0.348
90°	5	6	1.20×10^{-3}	5.68×10^{-2}	1.03×10^{-3}	0.559	0.324
90°	10	6	1.43×10^{-3}	7.23×10^{-2}	2.47×10^{-3}	0.467	0.500
70°	1	0	1.16×10^{-2}	8.77×10^{-2}	-	0.238	-
70°	5	0	1.00×10^{-2}	1.36×10^{-3}	-	0.286	-
70°	10	0	1.12×10^{-1}	8.30×10^{-1}	-	0.077	-
70°	1	1	6.45×10^{-3}	2.36×10^{-2}	-	0.222	-
70°	5	1	4.35×10^{-3}	8.92×10^{-2}	-	0.429	-
70°	10	1	1.60×10^{-2}	6.05×10^{-1}	-	-	-
70°	1	3	3.59×10^{-3}	1.07×10^{-2}	-	0.286	-
70°	5	3	2.66×10^{-3}	7.56×10^{-2}	-	0.875	-
70°	10	3	6.58×10^{-3}	1.12×10^{-1}	3.30×10^{-3}	0.375	0.500
70°	1	6	2.39×10^{-3}	1.15×10^{-2}	1.10×10^{-3}	0.750	0.700
70°	5	6	2.01×10^{-3}	6.90×10^{-2}	1.14×10^{-3}	1.182	0.559
70°	10	6	3.88×10^{-3}	2.26×10^{-2}	1.17×10^{-3}	0.700	1.150
70°	1	24	5.69×10^{-4}	4.28×10^{-3}	5.67×10^{-4}	0.800	0.917
70°	5	24	9.10×10^{-3}	1.36×10^{-3}	5.83×10^{-4}	1.091	1.000
70°	10	24	1.07×10^{-3}	7.57×10^{-3}	7.22×10^{-4}	0.957	0.714
70°	1	116	2.04×10^{-4}	4.71×10^{-3}	3.49×10^{-4}	0.889	0.391

Cooling rate - °C/min.

Isothermal time - hours

G - growth rate in μm/s

J - nucleation rate in $\mu m^3/s$

Table 3: Glass and MI Compositions for ΔT=90°

Isothermal Period = 0 hrs.						
	1°/min		5°/min		10°/min	
	Glass Avg	2σ	Glass Avg	2σ	Glass Avg	2σ
SiO_2	47.99	0.56	48.85	0.45	49.35	0.34
TiO_2	0.83	0.06	0.75	0.06	0.78	0.06
Al_2O_3	17.51	0.69	18.33	0.89	18.69	0.98
FeO*	7.03	0.20	6.52	0.22	6.37	0.32
MnO	0.11	0.02	0.13	0.03	0.12	0.03
MgO	9.06	0.29	9.32	0.39	9.03	0.47
CaO	14.62	0.14	14.79	0.12	14.73	0.13
Na_2O	1.57	0.06	1.40	0.06	1.51	0.05
K_2O	0.07	0.02	0.06	0.02	0.07	0.02
P_2O_5	0.05	0.01	0.06	0.01	0.05	0.01
Cr_2O_3	0.10	0.03	0.07	0.03	0.07	0.02
ZrO_2	0.06	0.05	0.07	0.05	0.06	0.05
	99.00	n=31	100.35	n=32	100.83	n=20
	Plag MI Avg	2σ	Plag MI Avg	2σ	Plag MI Avg	2σ
SiO_2	48.69		-		-	
TiO_2	0.95		-		-	
Al_2O_3	14.87		-		-	
FeO*	7.61		-		-	
MnO	0.12		-		-	
MgO	10.16		-		-	
CaO	14.58		-		-	
Na_2O	1.42		-		-	
K_2O	0.06		-		-	
P_2O_5	0.03		-		-	
Cr_2O_3	0.07		-		-	
ZrO_2	0.14		-		-	
	98.70	n=1		n=0		n=0

Isothermal Period = 6 hrs.						
	1°/min		5°/min		10°/min	
	Glass Avg	2σ	Glass Avg	2σ	Glass Avg	2σ
SiO_2	55.85	0.40	53.77	0.97	50.24	0.15
TiO_2	0.63	0.06	0.80	0.20	1.19	0.04
Al_2O_3	16.14	0.22	15.72	0.37	14.32	0.11
FeO*	5.58	0.39	6.12	0.57	7.41	0.12
MnO	0.13	0.04	0.12	0.02	0.14	0.02
MgO	9.71	0.15	9.82	0.13	9.56	0.13
CaO	11.27	0.23	12.12	0.32	15.24	0.13
Na_2O	0.88	0.02	0.92	0.10	1.19	0.03
K_2O	0.06	0.02	0.06	0.03	0.11	0.01
P_2O_5	0.07	0.05	0.08	0.01	0.09	0.01
Cr_2O_3	0.06	0.03	0.06	0.02	0.07	0.05
ZrO_2	n/a	n/a	n/a	n/a	n/a	n/a
	100.38	n=5	99.59	n=12	99.56	n=5
	Plag MI Avg	2σ	Plag MI Avg	2σ	Plag MI Avg	2σ
SiO_2	55.32	0.41	53.71	0.71	-	
TiO_2	0.68	0.10	0.76	0.27	-	
Al_2O_3	16.12	0.26	15.45	0.45	-	
FeO*	5.56	0.51	6.21	0.54	-	
MnO	0.11	0.03	0.11	0.02	-	
MgO	9.8	0.28	10.16	1.27	-	
CaO	11.43	0.33	11.93	0.57	-	
Na_2O	0.83	0.03	0.88	0.09	-	
K_2O	0.08	0.02	0.07	0.02	-	
P_2O_5	0.05	0.02	0.07	0.00	-	
Cr_2O_3	0.05	0.03	0.07	0.02	-	
ZrO_2	n/a	n/a	n/a	n/a	-	
	100.03	n=7	99.42	n=6		n=0

Table 3
continued

Isothermal Period = 6 hrs.		
	1°/min	
	Ol MI	
	Avg	**2σ**
SiO_2	56.09	0.73
TiO_2	0.65	0.04
Al_2O_3	16.57	0.23
FeO*	5.64	0.54
MnO	0.12	0.03
MgO	9.81	0.21
CaO	11.6	0.13
Na_2O	0.84	0.03
K_2O	0.04	0.02
P_2O_5	0.06	0.01
Cr_2O_3	0.07	0.03
ZrO_2	0.04	0.04
	101.53	n=9

Table 4: Glass and MI Compositions for $\Delta T=70^{o}$

Isothermal Period = 0 hrs.						
	1°/min Glass		**5°/min Glass**		**10°/min Glass**	
	Avg	**2σ**	**Avg**	**2σ**	**Avg**	**2σ**
SiO_2	48.82	0.35	49.35	0.42	49.22	0.33
TiO_2	0.85	0.03	0.86	0.07	0.80	0.07
Al_2O_3	18.63	0.36	18.51	1.00	18.74	1.07
FeO*	7.07	0.11	7.09	0.33	6.53	0.30
MnO	0.10	0.03	0.11	0.04	0.08	0.02
MgO	8.44	0.13	8.18	0.43	8.92	0.49
CaO	14.48	0.14	14.51	0.32	14.68	0.13
Na_2O	1.78	0.12	1.80	0.16	1.58	0.06
K_2O	0.05	0.01	0.06	0.01	0.05	0.01
P_2O_5	0.06	0.02	0.06	0.02	0.06	0.02
Cr_2O_3	0.09	0.04	0.11	0.03	0.07	0.02
ZrO_2	n/a	n/a	n/a	n/a	n/a	n/a
	100.37	n=15	100.64	n=17	100.73	n=16

Isothermal Period = 1 hr						
	1°/min Glass		**5°/min Glass**		**10°/min Glass**	
	Avg	**2σ**	**Avg**	**2σ**	**Avg**	**2σ**
SiO_2	49.51	0.19	50.61	0.29	50.11	0.55
TiO_2	0.94	0.02	1.06	0.03	0.89	0.07
Al_2O_3	16.7	0.09	16.54	0.11	17.99	1.05
FeO*	7.54	0.19	6.56	0.63	6.75	0.30
MnO	0.1	0.24	0.14	0.03	0.08	0.02
MgO	9.93	0.16	9.82	0.19	8.88	0.48
CaO	14.77	0.16	14.68	0.29	13.80	0.13
Na_2O	1.41	0.04	1.52	0.06	1.60	0.05
K_2O	0.06	0.01	0.06	0.01	0.06	0.01
P_2O_5	0.08	0.02	0.09	0.02	0.05	0.03
Cr_2O_3	0.1	0.03	0.12	0.02	0.05	0.02
ZrO_2	n/a	n/a	0.07	0.04	n/a	n/a
	101.14	n=10	101.27	n=16	100.26	n=10

	Plag MI Avg	**2σ**	**Plag MI Avg**	**2σ**	**Plag MI Avg**	**2σ**
SiO_2	48.84	0.19	-		-	
TiO_2	0.98	0.02	-		-	
Al_2O_3	16.97	0.89	-		-	
FeO*	7.49	0.12	-		-	
MnO	0.15	0.02	-		-	
MgO	8.93	0.30	-		-	
CaO	14.49	0.34	-		-	
Na_2O	1.82	0.06	-		-	
K_2O	0.05	0.01	-		-	
P_2O_5	0.11	0.01	-		-	
Cr_2O_3	0.13	0.02	-		-	
ZrO_2	n/a	n/a	-		-	
	99.96	n=3		n=0		n=0

	Plag MI Avg	**2σ**	**Plag MI Avg**	**2σ**	**Plag MI Avg**	**2σ**
SiO_2	-		50.51	0.52	-	
TiO_2	-		1.07	0.04	-	
Al_2O_3	-		16.36	0.50	-	
FeO*	-		6.91	0.62	-	
MnO	-		0.13	0.03	-	
MgO	-		9.79	0.28	-	
CaO	-		14.39	0.34	-	
Na_2O	-		1.51	0.05	-	
K_2O	-		0.07	0.01	-	
P_2O_5	-		0.10	0.03	-	
Cr_2O_3	-		0.13	0.02	-	
ZrO_2	-		0.11	0.05	-	
		n=0	101.08	n=7		n=0

Table 4 continued

Isothermal Period = 3 hrs.							Isothermal Period = 6 hrs.					
	1°/min Glass		5°/min Glass		10°/min Glass		1°/min Glass		5°/min Glass		10°/min Glass	
	Avg	2σ	Avg	2σ	Avg	2σ	Avg	2σ	Avg	2σ	Avg	2σ
SiO_2	50.04	0.23	50.49	0.33	49.88	0.34	53.49	0.48	51.73	0.53	50.63	0.54
TiO_2	1.00	0.04	1.00	0.04	0.95	0.02	0.39	0.02	0.78	0.03	0.68	0.05
Al_2O_3	16.39	0.47	16.61	0.09	16.64	0.13	18.91	0.23	17.05	0.20	17.61	1.12
FeO*	7.65	0.20	6.93	0.17	7.37	0.13	5.07	0.13	7.27	0.14	5.99	0.37
MnO	0.13	0.03	0.14	0.02	0.12	0.03	0.12	0.02	0.13	0.03	0.11	0.04
MgO	8.95	0.20	9.70	0.07	10.26	0.13	11.51	0.30	10.2	0.08	10.87	0.80
CaO	13.12	0.26	14.12	0.28	13.99	0.27	11.21	0.09	12.52	0.07	12.59	0.42
Na_2O	1.98	0.06	1.61	0.03	1.72	0.04	0.91	0.05	1.37	0.06	1.15	0.06
K_2O	0.12	0.01	0.08	0.00	0.05	0.01	0.04	0.01	0.08	0.01	0.06	0.01
P_2O_5	0.09	0.03	0.10	0.02	0.06	0.02	0.04	0.02	0.07	0.02	0.08	0.03
Cr_2O_3	0.09	0.04	0.12	0.01	0.07	0.03	0.06	0.03	0.09	0.03	0.07	0.03
ZrO_2	0.03	0.03	0.06	0.03	0.14	0.04	0.03	0.02	0.03	0.03	n/a	n/a
	99.59		100.96	n=9	101.25		101.78	n=12	101.32	n=9	99.84	n=29
	Plag MI		**Plag MI**		**Plag MI**		**Plag MI**		**Plag MI**		**Plag MI**	
	Avg	**2σ**	**Avg**	**2σ**	**Avg**	**2σ**	**Avg**	**2σ**	**Avg**	**2σ**	**Avg**	**2σ**
SiO_2	-		50.69	0.33	-		54.92	1.17	51.73	0.29	51.01	0.53
TiO_2	-		1.02	0.04	-		0.39	0.02	0.77	0.05	0.72	0.05
Al_2O_3	-		16.63	0.77	-		17.98	0.47	17.01	0.55	17.36	0.79
FeO*	-		6.89	0.13	-		4.79	0.36	7.20	0.20	5.95	0.18
MnO	-		0.15	0.03	-		0.09	0.01	0.13	0.02	0.12	0.05
MgO	-		9.67	0.49	-		11.18	0.39	10.16	0.21	10.96	0.72
CaO	-		14.41	0.31	-		11.06	0.17	12.7	0.23	12.88	0.26
Na_2O	-		1.59	0.02	-		0.94	0.06	1.35	0.04	1.12	0.08
K_2O	-		0.08	0.01	-		0.04	0.01	0.08	0.01	0.05	0.01
P_2O_5	-		0.11	0.03	-		0.02	0.00	0.05	0.08	0.08	0.01
Cr_2O_3	-		0.10	0.02	-		0.06	0.00	0.08	0.02	0.06	0.02
ZrO_2	-		0.07	0.03	-		0.06	0.04	0.04	0.02	n/a	n/a
		n=0	101.41	n=9		n=0	101.53	n=2	101.3	n=11	100.31	n=5

Table 4 continued

	Isothermal Period =24 hrs.						Isothermal Period =116 hrs.	
	1°/min Glass		5°/min Glass		10°/min Glass		1°/min Glass	
	Avg	2σ	Avg	2σ	Avg	2σ	Avg	2σ
Si	49.15	0.51	50.35	0.27	49.19	0.16	51.41	0.21
Ti	0.95	0.34	1.05	0.03	1.09	0.02	1.08	0.03
Al	17.62	0.49	15.96	0.12	15.55	0.09	15.13	0.07
Fe	6.52	1.97	6.01	0.23	7.75	0.10	5.73	0.13
Mn	0.12	0.06	0.15	0.02	0.13	0.03	0.14	0.04
Mg	9.83	0.57	10.53	0.07	10.24	0.04	10.48	0.06
Ca	14.83	0.82	14.22	0.15	14.56	0.13	14.31	0.11
Na	0.89	0.08	1.53	0.04	1.06	0.03	0.88	0.03
K	0.05	0.02	0.10	0.01	0.07	0.00	0.10	0.01
P	0.09	0.05	0.08	0.02	0.10	0.03	0.06	0.03
Cr	0.06	0.04	0.07	0.03	0.1	0.02	0.08	0.03
Zr	0.05	0.06	0.05	0.04	0.09	0.03	0.07	0.04
	100.16	n=5	100.1	n=8	99.93	n=8	99.47	n=8
	Plag MI		**Plag MI**		**Plag MI**		**Plag MI**	
	Avg	**2σ**	**Avg**	**2σ**	**Avg**	**2σ**	**Avg**	**2σ**
Si	49.02		-		49.32	0.25	50.87	0.89
Ti	1.08		-		1.07	0.01	1.03	0.06
Al	16.13		-		15.76	0.42	16.56	0.93
Fe	7.53		-		7.72	0.12	5.73	0.21
Mn	0.12		-		0.16	0.04	0.14	0.01
Mg	10.18		-		10.15	0.19	9.89	0.44
Ca	14.71		-		14.52	0.21	14.31	0.20
Na	0.85		-		1.06	0.01	0.92	0.02
K	0.06		-		0.08	0.00	0.10	0.01
P	0.02		-		0.11	0.01	0.11	0.04
Cr	0.03		-		0.09	0.00	0.09	0.00
Zr	0.00		-		0.07	0.04	0.07	0.06
	99.73	n=1		n=0	100.11	n=3	99.82	n=2

Table 4
continued

Isothermal Period = 6 hrs.

	1°/min Ol MI		5°/min Ol MI		10°/min Ol MI	
	Avg	**2σ**	**Avg**	**2σ**	**Avg**	**2σ**
SiO_2	54.23	0.81	50.48	1.19	50.96	0.54
TiO_2	0.38	0.05	0.70	0.09	0.71	0.04
Al_2O_3	18.26	0.97	17.07	1.71	17.53	0.35
FeO*	4.80	0.28	6.89	0.57	5.84	0.14
MnO	0.09	0.02	0.14	0.04	0.12	0.03
MgO	11.95	1.97	10.31	2.40	10.57	0.50
CaO	11.01	0.52	12.22	0.73	12.56	0.19
Na_2O	0.95	0.06	1.35	0.08	1.23	0.04
K_2O	0.03	0.01	0.08	0.02	0.07	0.01
P_2O_5	0.04	0.02	0.08	0.03	0.08	0.05
Cr_2O_3	0.10	0.03	0.08	0.03	0.07	0.03
ZrO_2	0.02	0.03	0.04	0.02	n/a	n/a
	101.86 n=16		99.44 n=8		1.45 n=8	

Isothermal Period =24 hrs.

	1°/min Ol MI		5°/min Ol MI		10°/min Ol MI	
	Avg	**2σ**	**Avg**	**2σ**	**Avg**	**2σ**
SiO_2	48.73		50.39	0.87	49.47	0.68
TiO_2	0.97		1.06	0.05	1.09	0.01
Al_2O_3	15.73		15.90	0.24	15.79	0.12
FeO*	8.21		5.81	0.38	7.21	0.80
MnO	0.17		0.16	0.02	0.1	0.00
MgO	10.79		10.60	0.17	10.03	0.01
CaO	14.52		14.10	0.19	14.38	0.31
Na_2O	0.88		1.54	0.07	1.17	0.09
K_2O	0.02		0.10	0.02	0.07	0.00
P_2O_5	0.10		0.09	0.03	0.12	0.01
Cr_2O_3	0.09		0.09	0.03	0.08	0.03
ZrO_2	0.07		0.06	0.02	0.03	0.05
	n=1		99.9 n=5		99.54 n=2	

Table 4 continued

Isothermal Period =116 hrs.		
	1°/min Ol MI Avg	**2σ**
SiO_2	50.61	0.80
TiO_2	1.09	0.02
Al_2O_3	15.25	0.29
FeO*	5.98	0.27
MnO	0.15	0.02
MgO	10.74	0.38
CaO	14.2	0.15
Na_2O	0.96	0.18
K_2O	0.10	0.01
P_2O_5	0.11	0.03
Cr_2O_3	0.09	0.02
ZrO_2	0.10	0.05
	99.38 n=5	

Table 5: Mineral Compositions

ΔT	Cooling rate	Isothermal time	Predicted An[a]	Predicted An[b]	Plag core An*	Plag rim An	Olivine Fo
90°	1	0	86.36	89.05	97.11	83.72	-
90°	1	6	83.06	92.01	88.28		91.35
90°	5	0	88.13	89.55	97.02	86.41	-
90°	5	6	83.47	87.88	85.95		-
90°	10	0	87.83	98.25	96.68		-
90°	10	6	82.72	87.95	87.82		89.10
70°	1	0	91.56	91.68	94.04	84.89	-
70°	1	1	90.17	90.97	94.72	86.29	-
70°	1	3	91.26	83.69	88.67		-
70°	1	6	92.77	93.00	89.08		93.76
70°	1	24	90.21	90.87	91.46		89.64
70°	1	116	89.06	90.24	88.84		91.77
70°	5	0	89.22	91.14	94.10	84.50	-
70°	5	1	86.99	89.05	89.72	83.51	-
70°	5	3	86.46	88.22	92.72	83.95	-
70°	5	6	87.57	92.40	87.04		91.33
70°	5	24	88.31	87.46	88.97		91.62
70°	10	0	90.92	94.09	95.55	93.70	-
70°	10	1	89.45	92.18	95.91	91.62	-
70°	10	3	86.16	86.81	95.11	88.47	94.20
70°	10	6	90.33	97.16	95.82	87.49	92.47
70°	10	24	89.29	93.37	89.68		89.61

Values are averages

*when no rim values are listed, no zoning was present and core values refer to averages for whole crystals

a Expected An values calculated with equation 1 of Panjasawatwong et al., (1995)

b Expected An values calculated with Danyushevsky routine in PETROLOG